

The hp nonconforming mesh refinement in discontinuous Galerkin finite element method based on Zienkiewicz-Zhu error estimation

Jan Jaśkowiec

Cracow University of Technology, Faculty of Civil Engineering

Institute for Computational Civil Engineering

Warszawska 24, 31-155 Kraków, Poland

e-mail: j.jaskowiec@L5.pk.edu.pl

This paper deals with hp -type adaptation in the discontinuous Galerkin (DG) method. The DG method is formulated in this paper with a non-zero mesh skeleton width, which leads to a version of the method called in this paper the interface discontinuous Galerkin (IDG) method. In this formulation, the mesh skeleton has a finite volume and special finite elements are used for discretization. The skeleton spatial calculations are performed using the finite difference or mid-values formulas which are based on the shape functions of the neighbouring finite elements. The Dirichlet boundary conditions are applied using a non-zero width of the material between the outer boundary and a finite element aligned with the boundary. Next, the paper discusses the mesh refinement of hp type. In the IDG method, the mesh does not have to be conforming. The Zienkiewicz-Zhu (ZZ) error indicator is adapted in the IDG method for the purpose of mesh refinement. The paper is illustrated with two-dimensional examples, in which the mesh refinement for an elliptic problem is performed.

Keywords: discontinuous Galerkin method, hp refinement, Zienkiewicz-Zhu error estimation.

1. INTRODUCTION

In this paper a formulation of the discontinuous Galerkin (DG) method which involves a finite element mesh skeleton with a non-zero thickness and afterwards the hp -type mesh refinement based on the adapted Zienkiewicz-Zhu (ZZ) error estimation are presented. In this approach, the mesh skeleton has a finite volume and creates a kind of interface between the neighbouring finite elements. This is why, in order to distinguish this approach from the standard discontinuous Galerkin (SDG) approach [3], the formulation presented in this paper is named the interface discontinuous Galerkin (IDG) method. The IDG method presented in this paper is an original approach. However, the idea that lies behind the IDG method has already been successfully developed and applied to XFEM modelling [31] or to coupling of finite element method with meshless method [30].

In this paper, the IDG method is applied to a scalar elliptic problem in three-dimensional (3D) domains. However, the examples presented in this paper are for two-dimensional cases. A typical example of scalar elliptic problem is heat transport, which has been chosen here for analysis. Although the paper is focused on elliptic problems, the approach can be directly applied to other kinds of problems.

The origin of the discontinuous Galerkin (DG) method goes back to 1970s [37], when the method was first introduced and applied to the numerical solution of a neutron transport PDE problem. The DG method has been subsequently explored since its introduction by many researchers and numerous DG methods have been developed, for example: the total variation bounded Runge-Kutta DG method [4, 11–13, 52], the local DG method [9, 10, 32], the interior penalty (IPDG)

method, the mixed DG method, the central DG method, the hybridizable DG method, the space-time DG method, the positivity-preserving DG method, and many others. The DG method has also been applied to some particular problems in structural mechanics, e.g., see [18, 28, 36], in fracture modeling [42, 43, 45] or in modeling of the phase flow in porous media [19, 40]. The DG method has been found sufficiently flexible for hp refinement and applicable to various partial differential equations, e.g. [5, 6, 23, 25, 53].

Various techniques are used in the DG method for *a posteriori* error estimation. For example, in [1] the computable *a posteriori* error bounds are obtained for the error measured in DG-norm and the broken energy seminorm. In, [20] the authors deal with convection-diffusion equations discretized with the non-symmetric interior penalty and the local discontinuous Galerkin methods in which *a posteriori* estimate obtained using duality technique and residual-based error estimators. The convection-diffusion problem is also considered in [26], but in this case a residual-based *a posteriori* error estimator is proposed that is subsequently applied for a fully automated hp -refinement. The hyperbolic problems were analysed in [29] for which the *a posteriori* error bounds were derived by employing a duality argument. In [33], as an error estimator the authors used a residual based error estimator that is applied to the convection dominated non-linear, quasi-stationary diffusion-convection-reaction equations. A survey concerning the error measure for the DG method in elliptic problems is presented in [41]. The Zienkiewicz-Zhu (ZZ) gradient recovery method presented in [55] has been applied in this paper for error estimation and, afterwards, for mesh refinement. The ZZ indicator is widely used in the standard finite element analysis [8, 54, 56, 57]. The gradient recovery approach is simple and quite effective, and this is why it is quite often used for mesh refinement, e.g., [22, 35]. The gradient recovery technique is unsuitable for the discontinuous Galerkin method, because of the discontinuous approximation fields, but there are some studies that try to tackle this problem [14, 44]. However, the ZZ method can be quite easily applied in the IDG method. In order to adapt the ZZ approach in the IDG method, the additional integrals over the mesh skeleton and outer boundary have to be considered. In this paper the mesh refinement is non-conforming in the sense that the so-called ‘hanging’ nodes may appear in the refinement procedure. This gives a great flexibility in mesh refinement because the refinement can be reduced to one single element without the necessity to disturb the neighbouring elements. Neither the approximation based on incremental hierarchical shape functions [17, 46, 50] nor the constrained approximation [16, 51], required in the locally p - and h -adaptive FEM, respectively, are necessary in IDG. Instead the so-called skeleton elements are employed, which are introduced in this paper. The effectiveness of the ZZ algorithm is shown in the examples in which the hp -type mesh refinement is performed on the IDG method solution.

The DG method on non-conforming meshes is a quite new research topic and there are not too many papers concerning this problem. In the DG methods, the mortar approach is applied [5, 34] or some techniques are used to stabilize the solution [7, 21, 24, 27]. In the IDG method, no special technique is needed in the case of mesh non-conformity. Due to the skeleton finite elements in the IDG method the problem with non-conforming mesh is naturally overcome.

The problem which is the focus of this paper is defined in the following Sec. 2. Section 3 presents formulation of the IDG method. Section 4 deals with boundary conditions in the IDG method. The IDG method is completed in Sec. 5 where the approximation is introduced which results in the algebraic system of equations. The details related to Zienkiewicz-Zhu error indicator are presented in Sec. 6. In Sec. 7 the refinement procedure is described. In the IDG method, the width of the mesh skeleton has to be properly evaluated and this is the topic of Sec. 8. The presented approach is illustrated with examples in Sec. 9. Finally, the paper ends with some conclusions.

2. FORMULATION OF THE PROBLEM

The IDG method is presented for an elliptic problem with the physical interpretation of stationary heat transport. The considered problem is defined in the domain Ω with outer boundary Γ . The

studied three-dimensional model starts with the well-known local form of heat flux balance equation, the Fourier law as well as essential and natural boundary conditions

$$\begin{aligned}
 \operatorname{div} \mathbf{q} &= r, & \text{in } \Omega, \\
 \mathbf{q} &= -k \nabla \Theta, & \text{in } \Omega, \\
 \Theta &= \widehat{\Theta}, & \text{on } \Gamma_{\Theta}, \\
 \mathbf{q} \cdot \mathbf{n} &= \widehat{h}, & \text{on } \Gamma_q,
 \end{aligned} \tag{1}$$

where Θ is the temperature field, \mathbf{q} the heat flux vector, r the heat source density, k is the heat conductivity parameter of a thermally isotropic material, $\widehat{\Theta}$ and \widehat{h} are prescribed values of temperature and heat flux, respectively, Γ_{Θ} and Γ_q are the parts of Γ where the temperature $\widehat{\Theta}$ and the heat flux \widehat{h} , respectively, are prescribed. The heat flux vector is connected with the temperature field by means of Fourier's law included in (1).

The problem in its strong formulation, Eq. (1), can be rewritten in the weak form with a v_{Θ} test function

$$\int_{\Omega} v_{\Theta} \operatorname{div} \mathbf{q} \, d\Omega - \int_{\Omega} v_{\Theta} r \, d\Omega = 0, \quad \forall v_{\Theta}. \tag{2}$$

When the integration by parts is performed on the first component in Eq. (2), it results in

$$\int_{\Gamma} v_{\Theta} \mathbf{q} \cdot \mathbf{n} \, d\Gamma - \int_{\Omega} \nabla v_{\Theta} \cdot \mathbf{q} \, d\Omega - \int_{\Omega} v_{\Theta} r \, d\Omega = 0, \quad \forall v_{\Theta}. \tag{3}$$

Equation (3) is the starting point for the IDG method which is presented in the next section.

3. FORMULATION OF THE INTERFACE DISCONTINUOUS GALERKIN METHOD

In order to obtain the approximate solution of the problem in Eq. (3) the domain under consideration is structured by a finite element mesh. The mesh consists of a set of cells (finite elements), nodes and inter-element borders. The set of the inter-element borders is called in this paper the finite element skeleton Γ_s , or skeleton in short. The cells, mesh skeleton and outer border are presented in Fig. 1, where the finite element mesh is constructed of these objects.

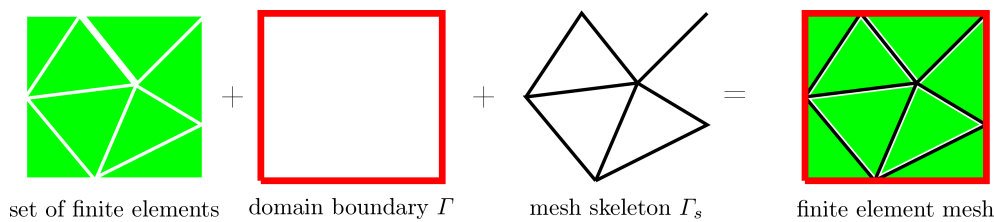


Fig. 1. Division of finite element mesh into: i) set of finite element interiors, ii) outer boundary Γ , iii) mesh skeleton Γ_s .

In the standard FEM, two adjacent elements share a common segment of the skeleton and also common nodes as well as degrees of freedom associated with those nodes. In the approach presented in this paper it is assumed that the skeleton has a non-zero width and each segment of the skeleton is discretized by a finite element. The skeleton finite element is rectangular in 2D or parallelepiped in 3D. In Fig. 2, the discretization together with the discretized skeleton are schematically depicted. As can be seen in this figure, the regular finite elements are diminished adequately to the width of the skeleton. The skeleton finite elements play a role of inter-element interfaces that can 'glue' together the regular finite elements of different order or join together the non-conforming finite elements, which is shown in Fig. 3.

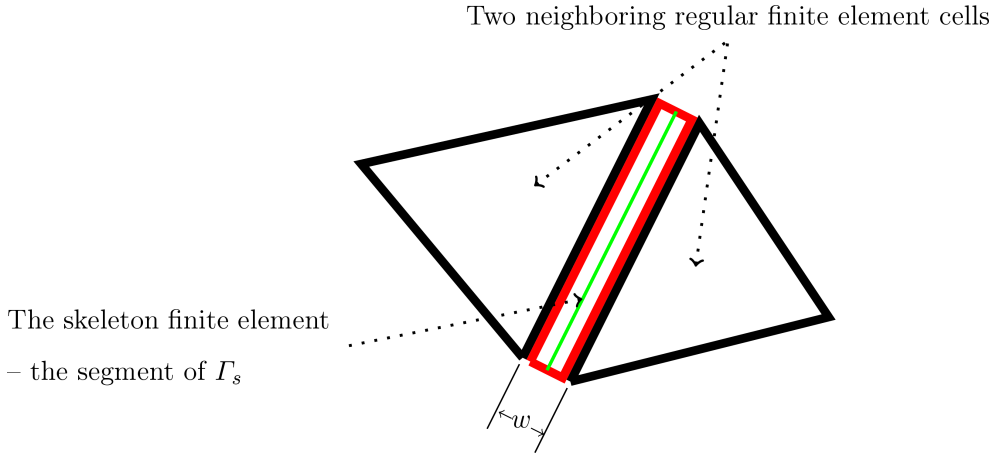


Fig. 2. The configuration of two neighbouring finite element cells with the skeleton finite element of width w .

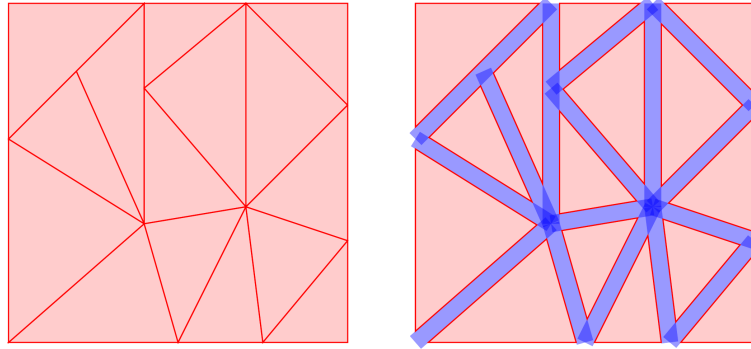


Fig. 3. Example of non-conforming finite element cells with the skeleton finite elements.

The domain volume Ω can be expressed as the sum of the volumes of all the regular finite elements Ω_E and the skeleton volume Ω_s

$$\Omega = \Omega_E \cup \Omega_s, \quad \Omega_E \cap \Omega_s = \emptyset. \quad (4)$$

The skeleton volume, on the other hand, can be expressed by the mesh skeleton Γ_s and its width w :

$$\Omega_s = \Gamma_s \times w. \quad (5)$$

In the regular finite elements, the construction of shape functions and the integration schemes are performed in a standard way. However, the skeleton finite elements are treated in a special way, regarding interpolations, integrations and assembling procedures. By definition, the skeleton finite elements are very thin, which is why all the computations regarding those elements are performed in the so-called skeleton local coordinates $(\mathbf{n}^s, \mathbf{s}^s, \mathbf{r}^s)$, where \mathbf{n}^s is unit vector normal to skeleton segment, and \mathbf{s}^s and \mathbf{r}^s are mutually perpendicular unit vectors that are tangent to the skeleton segment. In 2D, the local coordinates are reduced to two unit vectors, namely $(\mathbf{n}^s, \mathbf{s}^s)$. The orientation of the skeleton local coordinates is in fact arbitrary, providing that it meets the requirements stated above.

Remembering the relation in Eq. (4) the integrals over volume Ω from Eq. (3) can be written as the sum over these two volumes:

$$\int_{\Gamma} v_{\Theta} \mathbf{q} \cdot \mathbf{n} d\Gamma - \int_{\Omega_E} \nabla v_{\Theta} \cdot \mathbf{q} d\Omega - \int_{\Omega_s} \nabla v_{\Theta} \cdot \mathbf{q} d\Omega - \int_{\Omega_E} v_{\Theta} r d\Omega - \int_{\Omega_s} v_{\Theta} r d\Omega = 0. \quad (6)$$

Furthermore, on the basis of Eq. (5) the integrals over the mesh skeleton can be expressed as the integrals over the skeleton surface Γ_s and over the skeleton width w :

$$\int_{\Gamma} v_{\Theta} \mathbf{q} \cdot \mathbf{n} d\Gamma - \int_{\Omega_E} \nabla v_{\Theta} \cdot \mathbf{q} d\Omega - \int_{\Gamma_s} \int_w \nabla v_{\Theta} \cdot \mathbf{q} dw d\Gamma - \int_{\Omega_E} v_{\Theta} r d\Omega - \int_{\Gamma_s} \int_w v_{\Theta} r dw d\Gamma = 0. \quad (7)$$

On the basis of the assumption that the skeleton width w is very small (about thousands of times smaller than the size of the adjacent elements), the integrals over w can be expressed as a product of the skeleton width and the value of the integral over the skeleton surface:

$$\int_{\Gamma} v_{\Theta} \mathbf{q} \cdot \mathbf{n} d\Gamma - \int_{\Omega_E} \nabla v_{\Theta} \cdot \mathbf{q} d\Omega - \int_{\Gamma_s} w \nabla v_{\Theta} \cdot \mathbf{q} d\Gamma - \int_{\Omega_E} v_{\Theta} r d\Omega - \int_{\Gamma_s} w v_{\Theta} r d\Gamma = 0. \quad (8)$$

The third integral in (8) is over the skeleton surface, and in this integral the scalar product of the test function gradient and the heat flux vector have to be calculated on the skeleton surface Γ_s . The scalar product can be calculated in the global coordinates as well as in the skeleton local coordinates:

$$\nabla v_{\Theta} \cdot \mathbf{q} = \frac{\partial v_{\Theta}}{\partial x} q_x + \frac{\partial v_{\Theta}}{\partial y} q_y + \frac{\partial v_{\Theta}}{\partial z} q_z = \frac{\partial v_{\Theta}}{\partial n} q_n + \frac{\partial v_{\Theta}}{\partial s} q_s + \frac{\partial v_{\Theta}}{\partial r} q_r \quad \text{for } \mathbf{x} \in \Gamma_s, \quad (9)$$

where $\frac{\partial v_{\Theta}}{\partial n}$, $\frac{\partial v_{\Theta}}{\partial s}$ and $\frac{\partial v_{\Theta}}{\partial r}$ are the partial derivatives in \mathbf{n}^s , \mathbf{s}^s and \mathbf{r}^s directions, respectively, and q_n , q_s and q_r are the components of the heat flux vector in the skeleton local coordinates.

The skeleton finite elements are not typical because there are no standard shape functions in the elements. As can be seen in Eq. (8), the integrals concerning the skeleton finite elements are limited to the integrals along the skeleton segments. In order to compute this kind of integrals, we need to have approximation of required quantities just in the segment points, i.e., on the mid-surface of the skeleton elements. This is achieved by the values on both sides of the skeleton finite elements. As a result in the last integral in (8), the test function v_{Θ} is expressed as a mean value: $v_{\Theta} = \langle v_{\Theta} \rangle$. On the other hand, the derivatives in the skeleton normal direction can then be approximated with the help of the finite difference expression regarding Fourier's law, namely

$$q_n = -k \frac{[[\Theta]]}{w}, \quad \frac{\partial v_{\Theta}}{\partial n} = \frac{[[v_{\Theta}]]}{w}, \quad (10)$$

where the operators $[[\cdot]]$ and $\langle \cdot \rangle$ are defined as follows:

$$\begin{aligned} [[f]](\mathbf{x}) &= f(\mathbf{x} + 0.5 w \mathbf{n}^s) - f(\mathbf{x} - 0.5 w \mathbf{n}^s) = f^+(\mathbf{x}) - f^-(\mathbf{x}) \\ \langle f \rangle(\mathbf{x}) &= 0.5 \cdot (f^+(\mathbf{x}) + f^-(\mathbf{x})) \end{aligned} \quad \text{for } \mathbf{x} \in \Gamma_s. \quad (11)$$

The other components of the inner product in Eq. (9) are approximated by mid-values. Keeping in mind Fourier's law, the scalar product in Eq. (9) can now be written in the following form:

$$\nabla v_{\Theta} \cdot \mathbf{q} = -\frac{k}{w^2} [[v_{\Theta}]] [[\Theta]] - k \left\langle \frac{\partial v_{\Theta}}{\partial s} \right\rangle \left\langle \frac{\partial \Theta}{\partial s} \right\rangle - k \left\langle \frac{\partial v_{\Theta}}{\partial r} \right\rangle \left\langle \frac{\partial \Theta}{\partial r} \right\rangle \quad \text{for } \mathbf{x} \in \Gamma_s. \quad (12)$$

The derivatives in \mathbf{s}^s and \mathbf{r}^s directions from Eq. (12) can be written by means of gradients in the global coordinates, and this results in

$$\begin{aligned} \left\langle \frac{\partial v_{\Theta}}{\partial s} \right\rangle &= \langle \nabla v_{\Theta} \rangle \cdot \mathbf{s}^s, & \left\langle \frac{\partial v_{\Theta}}{\partial r} \right\rangle &= \langle \nabla v_{\Theta} \rangle \cdot \mathbf{r}^s, \\ \left\langle \frac{\partial \Theta}{\partial s} \right\rangle &= \langle \nabla \Theta \rangle \cdot \mathbf{s}^s, & \left\langle \frac{\partial \Theta}{\partial r} \right\rangle &= \langle \nabla \Theta \rangle \cdot \mathbf{r}^s. \end{aligned} \quad (13)$$

Finally, the scalar product in Eq. (12) is expressed by the values of temperature, test function and their gradients on the edges of neighbouring regular finite elements

$$\begin{aligned} \nabla v_{\Theta} \cdot \mathbf{q} &= -\frac{k}{w^2} [[v_{\Theta}]] [[\Theta]] - k \langle \nabla v_{\Theta} \rangle \cdot \mathbf{s}^s \otimes \mathbf{s}^s \cdot \langle \nabla \Theta \rangle - k \langle \nabla \rangle v_{\Theta} \cdot \mathbf{r}^s \otimes \mathbf{r}^s \cdot \langle \nabla \Theta \rangle \\ &= -\frac{k}{w^2} [[v_{\Theta}]] [[\Theta]] - k \langle \nabla v_{\Theta} \rangle \cdot (\mathbf{s}^s \otimes \mathbf{s}^s + \mathbf{r}^s \otimes \mathbf{r}^s) \cdot \langle \nabla \Theta \rangle \\ &= -\frac{k}{w^2} [[v_{\Theta}]] [[\Theta]] - k \langle \nabla v_{\Theta} \rangle \cdot \mathbf{Q}_{sr} \cdot \langle \nabla \Theta \rangle \quad \text{for } \mathbf{x} \in \Gamma_s, \end{aligned} \quad (14)$$

where \mathbf{Q}_{sr} is defined as

$$\mathbf{Q}_{sr} = \mathbf{s}^s \otimes \mathbf{s}^s + \mathbf{r}^s \otimes \mathbf{r}^s = \mathbf{I} - \mathbf{n}^s \otimes \mathbf{n}^s. \quad (15)$$

Substituting relation in Eq. (14) into Eq. (8) in the weak form, we obtain the following result:

$$\begin{aligned} \int_{\Gamma} v_{\Theta} \mathbf{q} \cdot \mathbf{n} \, d\Gamma + \int_{\Omega_E} k \nabla v_{\Theta} \cdot \nabla \Theta \, d\Omega + \int_{\Gamma_s} \frac{k}{w} [[v_{\Theta}]] [[\Theta]] \, d\Gamma \\ + \int_{\Gamma_s} w k \langle \nabla v_{\Theta} \rangle \cdot \mathbf{Q}_{sr} \cdot \langle \nabla \Theta \rangle \, d\Gamma - \int_{\Omega_E} v_{\Theta} r \, d\Omega - \int_{\Gamma_s} w \langle v_{\Theta} \rangle r \, d\Gamma = 0. \end{aligned} \quad (16)$$

In order to compare Eq. (16) with the adequate equation obtained in SDG [3], such an equation is presented below

$$\begin{aligned} \int_{\Gamma} v_{\Theta} \mathbf{q} \cdot \mathbf{n} \, d\Gamma + \int_{\Omega} k \nabla v_{\Theta} \cdot \nabla \Theta \, d\Omega + \int_{\Gamma_s} \sigma [[v_{\Theta}]] \cdot [[\Theta]] \, d\Gamma \\ - \int_{\Gamma_s} k [[v_{\Theta}]] \cdot \langle \nabla \Theta \rangle \, d\Gamma + \kappa \int_{\Gamma_s} k \langle \nabla v_{\Theta} \rangle \cdot [[\Theta]] \, d\Gamma - \int_{\Omega} v_{\Theta} r \, d\Omega = 0, \end{aligned} \quad (17)$$

where σ is the so-called discontinuity penalisation parameter. The σ parameter is taken to be of order $O(h^{-1})$, where h is the characteristic element size in a mesh, e.g., see [47, 48]. This parameter is set in this paper as $\sigma = \frac{\sigma_0}{h^2}$ where σ_0 is constant. The value of the penalisation parameter is assessed to be large enough to enforce continuity of the solution and, on the other hand, not too large to avoid numerical instabilities. The κ parameter has the values +1, -1 or 0. Depending on these values the following DG schemes arise:

- $\kappa = -1$ – symmetric interior penalty Galerkin (SIPG) [49],
- $\kappa = 1$ – nonsymmetric interior penalty Galerkin (NIPG) [39],
- $\kappa = 0$ – incomplete interior penalty Galerkin (IIPG) [15].

It can be noticed that in Eq. (16), obtained by the IDG method, the fourth and sixth integrals are new in comparison to the standard approach. On the other hand, in the SDG method the fourth and fifth integrals in Eq. (17) do not appear in Eq. (16). The third integrals in Eqs. (16) and (17) are quite similar, except the penalty parameter, which in Eq. (16) is substituted by k/w .

4. BOUNDARY CONDITIONS

The boundary conditions of Neumann and Dirichlet types, which are defined in Eq. (1), are written in Eq. (16) by means of the integral over the whole outer boundary Γ , i.e., $\int_{\Gamma} v_{\Theta} \mathbf{q} \cdot \mathbf{n} \, d\Gamma$. The Dirichlet boundary condition can be applied in a way typical of FEM, i.e., by assigning appropriate

values to degrees of freedom on the nodes on the Γ_Θ boundary. However, a different approach has been chosen in this paper, which is based on the integral along Γ_Θ .

The integral along the outer boundary can be written as the sum of two integrals: over Γ_q and Γ_Θ , and the Neumann boundary condition can be directly substituted here:

$$\int_{\Gamma} v_\Theta \mathbf{q} \cdot \mathbf{n} \, d\Gamma = \int_{\Gamma_q} v_\Theta \widehat{h} \, d\Gamma + \int_{\Gamma_\Theta} v_\Theta \mathbf{q} \cdot \mathbf{n} \, d\Gamma. \quad (18)$$

In order to apply the Dirichlet boundary conditions, it is assumed that along Γ_Θ there is a thin layer of material between the boundary and the regular finite elements, which is discretized by the skeleton finite element of the $\frac{1}{2}w$ width. Under these assumptions, the normal part of the heat flux can be expressed with the help of Fourier's law:

$$\mathbf{q} \cdot \mathbf{n} = q_n = -k \frac{\widehat{\Theta} - \Theta}{\frac{1}{2}w} = -2k \frac{\widehat{\Theta}}{w} + 2k \frac{\Theta}{w} \quad \text{on } \Gamma_\Theta. \quad (19)$$

Equations (18) and (19) are substituted to Eq. (16), as a result the weak form equation changes to the final form, in which both kind of boundary conditions are considered:

$$\begin{aligned} \int_{\Gamma_q} v_\Theta \widehat{h} \, d\Gamma - 2 \int_{\Gamma_\Theta} v_\Theta \frac{k}{w} \widehat{\Theta} \, d\Gamma + 2 \int_{\Gamma_\Theta} \frac{k}{w} v_\Theta \Theta \, d\Gamma + \int_{\Omega_E} k \nabla v_\Theta \cdot \nabla \Theta \, d\Omega + \int_{\Gamma_s} \frac{k}{w} [[v_\Theta]] [[\Theta]] \, d\Gamma \\ + \int_{\Gamma_s} w k \langle \nabla v_\Theta \rangle \cdot \mathbf{Q}_{sr} \cdot \langle \nabla \Theta \rangle \, d\Gamma - \int_{\Omega_E} v_\Theta r \, d\Omega - \int_{\Gamma_s} w \langle v_\Theta \rangle r \, d\Gamma = 0. \end{aligned} \quad (20)$$

Equation (20) can be written in the form of equality of bilinear and linear forms

$$A(\Theta, v_\Theta) = F(v_\Theta), \quad \forall v_\Theta, \quad (21)$$

where

$$\begin{aligned} A(\Theta, v_\Theta) = \int_{\Omega_E} k \nabla v_\Theta \cdot \nabla \Theta \, d\Omega + \int_{\Gamma_s} \frac{k}{w} [[v_\Theta]] [[\Theta]] \, d\Gamma \\ + \int_{\Gamma_s} w k \langle \nabla v_\Theta \rangle \cdot \mathbf{Q}_{sr} \cdot \langle \nabla \Theta \rangle \, d\Gamma + 2 \int_{\Gamma_\Theta} \frac{k}{w} v_\Theta \Theta \, d\Gamma, \end{aligned} \quad (22)$$

$$F(v_\Theta) = \int_{\Omega_E} v_\Theta r \, d\Omega + \int_{\Gamma_s} w \langle v_\Theta \rangle r \, d\Gamma - \int_{\Gamma_q} v_\Theta \widehat{h} \, d\Gamma + 2 \int_{\Gamma_\Theta} \frac{k}{w} v_\Theta \widehat{\Theta} \, d\Gamma.$$

5. APPROXIMATION

In order to solve Eq. (21), the solution function (temperature Θ) and the test function have to be approximated. The Bubnov-Galerkin approach is selected for this approximation, which means that both of the functions are approximated in the same manner. The approximation on Ω_E is done in a similar way as in the standard FEM, but now the shape functions are not continuous along adjacent regular finite elements.

The approximation in the e -th single regular finite element Ω^e is constructed with the help of the local basis functions and the local degrees of freedom

$$\Theta^e = \Phi_\Theta^e \check{\Theta}^e \quad \text{in } \Omega^e, \quad (23)$$

where Φ_{Θ}^e is the matrix of shape functions for the e -th element and $\check{\Theta}^e$ is the vector of local degrees of freedom associated with the e -th regular element. The matrix of shape functions Φ_{Θ}^e is the same as in FEM and their support is limited to Ω^e . Using the approximation in (23), the global approximation can be constructed that considers all the regular finite elements Ω_E

$$\Theta = \Phi_{\Theta} \check{\Theta} \quad \text{in } \Omega_E, \quad (24)$$

where

$$\Phi_{\Theta} = [\Phi_{\Theta}^1 \quad \Phi_{\Theta}^2 \quad \dots \quad \Phi_{\Theta}^N], \quad \check{\Theta} = \begin{bmatrix} \check{\Theta}^1 \\ \check{\Theta}^2 \\ \vdots \\ \check{\Theta}^N \end{bmatrix} \quad (25)$$

and N is the number of regular finite element cells.

It can be noticed that approximation in Eq. (24) takes into account the approximation of regular finite elements. Due to the fact that the skeleton finite elements are very thin, they can be neglected in the spatial discretization. However, the existence of skeleton finite elements is already taken into account in Eqs. (21) and (22).

The temperature gradient is approximated by the shape functions gradients

$$\nabla \Theta = \mathbf{B}_{\Theta} \check{\Theta} \quad \text{on } \Omega_E, \quad (26)$$

where $\mathbf{B}_{\Theta} = \nabla \Phi_{\Theta}$.

In the integrals over Γ_s the temperature jumps or mean-values are required, which are obtained by the following approximations

$$[[\Theta]] = [[\Phi_{\Theta}]] \check{\Theta}, \quad \langle \Theta \rangle = \langle \Phi_{\Theta} \rangle \check{\Theta}, \quad \langle \nabla \Theta \rangle = \langle \mathbf{B}_{\Theta} \rangle \check{\Theta} \quad \text{on } \Gamma_s. \quad (27)$$

For example, let us suppose that there are two neighbouring regular finite elements and we want to calculate the jump or mean values of matrix of shape functions at point \mathbf{x}_s that belong to the skeleton segment, see Fig. 4. Then the jump and mean value of shape functions matrix reads:

$$\begin{aligned} [[\Phi_{\Theta}]](\mathbf{x}_s) &= [\mathbf{0} \quad \dots \quad -\Phi_{\Theta}^{e1}(\mathbf{x}_s^-) \quad \dots \quad \mathbf{0} \quad \dots \quad \Phi_{\Theta}^{e2}(\mathbf{x}_s^+) \quad \dots \quad \mathbf{0}], \\ \langle \Phi_{\Theta} \rangle(\mathbf{x}_s) &= 0.5 [\mathbf{0} \quad \dots \quad \Phi_{\Theta}^{e1}(\mathbf{x}_s^-) \quad \dots \quad \mathbf{0} \quad \dots \quad \Phi_{\Theta}^{e2}(\mathbf{x}_s^+) \quad \dots \quad \mathbf{0}]. \end{aligned} \quad (28)$$

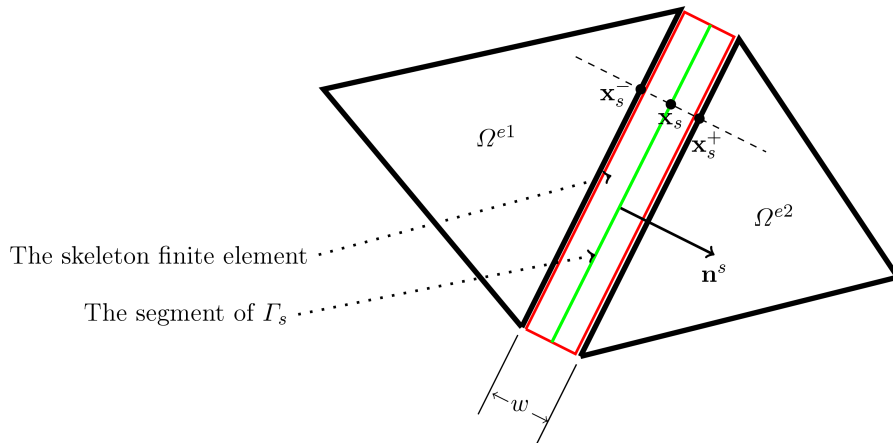


Fig. 4. Illustration of point positions to calculate the jump or mean values of shape functions of two neighbouring regular finite elements.

When the approximations in equations from (24) to (27) are substituted to Eq. (21), the linear system of equation is obtained:

$$\mathbf{K}\tilde{\Theta} = \mathbf{F}, \quad (29)$$

where

$$\begin{aligned} \mathbf{K} = & \int_{\Omega_E} k \mathbf{B}_\Theta^T \mathbf{B}_\Theta \, d\Omega + \int_{\Gamma_s} \frac{k}{w} [[\Phi_\Theta]]^T [[\Phi_\Theta]] \, d\Gamma \\ & + \int_{\Gamma_s} wk \langle \mathbf{B}_\Theta \rangle^T \mathbf{Q}_{sr} \langle \mathbf{B}_\Theta \rangle \, d\Gamma + 2 \int_{\Gamma_\Theta} \frac{k}{w} \Phi_\Theta^T \Phi_\Theta \, d\Gamma, \quad (30) \\ \mathbf{F} = & \int_{\Omega_E} \Phi_\Theta^T r \, d\Omega + \int_{\Gamma_s} \langle \Phi_\Theta \rangle^T w r \, d\Gamma - \int_{\Gamma_q} \Phi_\Theta^T \widehat{h} \, d\Gamma + 2 \int_{\Gamma_\Theta} \Phi_\Theta^T \frac{k}{w} \widehat{\Theta} \, d\Gamma \end{aligned}$$

It should be noted that the approximations presented in Eqs. (24)–(26) are common for the IDG and SDG methods. On the other hand, the approximations in Eq. (27) are true only for the IDG method due the different definition of the jump mid-value operators in comparison to the SDG method (see [38]).

6. THE ZIENKIEWICZ-ZHU INDICATOR

Zienkiewicz and Zhu introduced in [55] the so-called ZZ error indicator which has been applied to an elasticity problem. In this paper, the ZZ estimator is used for a heat transport problem using the discontinuous approximation, as presented in Sec. 5.

In the standard procedure, the ZZ error estimation is based on the integral over the whole domain, which is performed by the sum of integrals over all the finite elements. In the version of ZZ error estimation which is applied in this paper, the integral over the whole domain is written as the sum of integrals over all the regular finite elements volume Ω_E and over the mesh skeleton volume Ω_s . The integrals over Ω_s are treated in the same manner as in Eq. (8), i.e., as the integrals over Γ_s and the integrand multiplied by w . In the ZZ approach, the outer boundary is also treated as a skeleton but with a $\frac{1}{2}w$ width. In such a case, the ZZ error estimator in the version applied in this paper is based on the following error measure:

$$\epsilon = \frac{1}{|\Omega_E|} \int_{\Omega_E} (\mathbf{q} - \mathbf{q}^h)^T (\mathbf{q} - \mathbf{q}^h) \, d\Omega + \frac{1}{|\Omega_s|} \int_{\Omega_s} (\mathbf{q} - \mathbf{q}^h)^T (\mathbf{q} - \mathbf{q}^h) \, d\Omega, \quad (31)$$

where \mathbf{q} is the exact heat flux vector and \mathbf{q}^h is the approximated heat flux vector defined as $\mathbf{q}^h = -k \mathbf{B}_\Theta \tilde{\Theta}$, where $|\Omega_E|$ and $|\Omega_s|$ are the volumes of Ω_E and Ω_s subdomains. In the ZZ approach, the exact flux vector is substituted by the so-called smoothed vector \mathbf{q}^*

$$\epsilon_{zz} = \frac{1}{|\Omega_E|} \int_{\Omega_E} (\mathbf{q}^* - \mathbf{q}^h)^T (\mathbf{q}^* - \mathbf{q}^h) \, d\Omega + \frac{1}{|\Omega_s|} \int_{\Omega_s} (\mathbf{q}^* - \mathbf{q}^h)^T (\mathbf{q}^* - \mathbf{q}^h) \, d\Omega. \quad (32)$$

The vector \mathbf{q}^* is unknown at this stage of the analysis and set in such a way as to minimize the ϵ_{zz} error.

After taking into account Eq. (5) the second integral in Eq. (32) can be written in the following form:

$$\int_{\Omega_s} (\mathbf{q}^* - \mathbf{q}^h)^T (\mathbf{q}^* - \mathbf{q}^h) \, d\Omega = \int_{\Gamma_s} \int_{-\frac{w}{2}}^{\frac{w}{2}} (\mathbf{q}^* - \mathbf{q}^h)^T (\mathbf{q}^* - \mathbf{q}^h) \, d\tilde{w} \, d\Gamma, \quad (33)$$

where \tilde{w} is the auxiliary scalar variable that is used for integration along the skeleton thickness. The skeleton width is very small, thus it can be assumed that the heat flux changes linearly across the skeleton. The inner integral can be numerically calculated using two-point Gauss' integration rule without the loss of accuracy, that is

$$\begin{aligned} \int_{\Gamma_s} \int_{-\frac{w}{2}}^{\frac{w}{2}} (\mathbf{q}^* - \mathbf{q}^h)^\top (\mathbf{q}^* - \mathbf{q}^h) d\tilde{w} d\Gamma \\ = \int_{\Gamma_s} \frac{w}{2} \left((\mathbf{q}^* - \mathbf{q}^h)^\top (\mathbf{q}^* - \mathbf{q}^h) \right) \Big|_{\tilde{w}_1} + \frac{w}{2} \left((\mathbf{q}^* - \mathbf{q}^h)^\top (\mathbf{q}^* - \mathbf{q}^h) \right) \Big|_{\tilde{w}_2} d\Gamma, \end{aligned} \quad (34)$$

where \tilde{w}_1, \tilde{w}_2 are the Gauss integration points that read

$$\tilde{w}_1 = -\frac{w}{2} \frac{1}{\sqrt{3}}, \quad \tilde{w}_2 = \frac{w}{2} \frac{1}{\sqrt{3}}. \quad (35)$$

The smoothed heat flux is approximated with the same discontinuous shape functions as for the temperature field in (24), but now we need to remember that the heat flux is a vector

$$\mathbf{q}^* = \mathbf{\Phi}_q \check{\mathbf{q}}^*, \quad (36)$$

where $\check{\mathbf{q}}^*$ is the vector of degrees of freedom for the smoothed heat flux \mathbf{q}^* . The matrix of shape functions for the flux vector $\mathbf{\Phi}_q$ is constructed in similar manner as shown in Eqs. (23) to (25), but now for the flux vector. Equation (36) can be rewritten for each component of the vector \mathbf{q}^* , then the same matrix of shape functions as for temperature can be used

$$q_\alpha^* = \mathbf{\Phi}_\Theta \check{\mathbf{q}}_\alpha^*, \quad \alpha = x, y, z. \quad (37)$$

However, the approximation presented in Eq. (36) is used for the further analysis.

The vector of smoothed heat flux field degrees of freedom $\check{\mathbf{q}}^*$ can now be calculated by minimising the error in Eq. (32)

$$\frac{\partial \epsilon_{zz}}{\partial \check{\mathbf{q}}^*} = \mathbf{0} \quad \Rightarrow \quad \mathbf{M} \check{\mathbf{q}}^* = \mathbf{Z}, \quad (38)$$

where matrix \mathbf{M} and vector \mathbf{Z} are defined as follows:

$$\mathbf{M} = \int_{\Omega_E} \mathbf{\Phi}_q^\top \mathbf{\Phi}_q d\Omega + \int_{\Gamma_s} \frac{w}{2} \left(\mathbf{\Phi}_q^\top \mathbf{\Phi}_q \right) \Big|_{\tilde{w}_1} + \frac{w}{2} \left(\mathbf{\Phi}_q^\top \mathbf{\Phi}_q \right) \Big|_{\tilde{w}_2} d\Gamma. \quad (39)$$

On the basis of Eq. (11) it can be easily noticed that

$$\mathbf{\Phi}_q \Big|_{\tilde{w}_1} = s_1 \mathbf{\Phi}_q^- + s_2 \mathbf{\Phi}_q^+, \quad \mathbf{\Phi}_q \Big|_{\tilde{w}_2} = s_2 \mathbf{\Phi}_q^- + s_1 \mathbf{\Phi}_q^+, \quad (40)$$

where $s_1 = \frac{\sqrt{3}+1}{2\sqrt{3}}$, $s_2 = 1 - s_1$. In consequence, the matrix \mathbf{M} in Eq. (39) has the form

$$\begin{aligned} \mathbf{M} = \int_{\Omega_E} \mathbf{\Phi}_q^\top \mathbf{\Phi}_q d\Omega + \int_{\Gamma_s} \frac{w}{2} (s_1 \mathbf{\Phi}_q^- + s_2 \mathbf{\Phi}_q^+)^\top (s_1 \mathbf{\Phi}_q^- + s_2 \mathbf{\Phi}_q^+) d\Gamma \\ + \int_{\Gamma_s} \frac{w}{2} (s_2 \mathbf{\Phi}_q^- + s_1 \mathbf{\Phi}_q^+)^\top (s_2 \mathbf{\Phi}_q^- + s_1 \mathbf{\Phi}_q^+) d\Gamma. \end{aligned} \quad (41)$$

The right-hand side vector in Eq. (38) is defined in the following way:

$$\begin{aligned} \mathbf{Z} = & - \int_{\Omega_E} k \Phi_q^T \mathbf{B}_\Theta d\Omega \check{\Theta} - \int_{\Gamma_s} k \frac{w}{2} (s_1 \Phi_q^- + s_2 \Phi_q^+)^T (s_1 \mathbf{B}_\Theta^- + s_2 \mathbf{B}_\Theta^+) d\Gamma \check{\Theta} \\ & - \int_{\Gamma_s} k \frac{w}{2} (s_2 \Phi_q^- + s_1 \Phi_q^+)^T (s_2 \mathbf{B}_\Theta^- + s_1 \mathbf{B}_\Theta^+) d\Gamma \check{\Theta}. \end{aligned} \quad (42)$$

The system of equation in Eq. (38) with definitions in Eqs. (41) and (42) has a nice compact form for all coefficients of the flux vector \mathbf{q}^* . However, its size is thrice the size of the problem in Eq. (29). It can be easily noticed, keeping in mind the approximation in Eq. (37), that Eq. (38) can be rewritten as three independent sets of equations for each component of the heat flux vector

$$\mathbf{M}^\alpha \check{\mathbf{q}}_\alpha^* = \mathbf{Z}^\alpha, \quad \alpha = x, y, z, \quad (43)$$

where

$$\begin{aligned} \mathbf{M}^x = \mathbf{M}^y = \mathbf{M}^z = & \int_{\Omega_E} \Phi_\Theta^T \Phi_\Theta d\Omega + \int_{\Gamma_s} \frac{w}{2} (s_1 \Phi_\Theta^- + s_2 \Phi_\Theta^+)^T (s_1 \Phi_\Theta^- + s_2 \Phi_\Theta^+) d\Gamma \\ & + \int_{\Gamma_s} \frac{w}{2} (s_2 \Phi_\Theta^- + s_1 \Phi_\Theta^+)^T (s_2 \Phi_\Theta^- + s_1 \Phi_\Theta^+) d\Gamma, \end{aligned} \quad (44)$$

and

$$\begin{aligned} \mathbf{Z}^\alpha = & - \int_{\Omega_E} \mathbf{k} \Phi_\Theta^T \mathbf{B}_\Theta^\alpha d\Omega \check{\Theta} - \int_{\Gamma_s} k \frac{w}{2} (s_1 \Phi_\Theta^- + s_2 \Phi_\Theta^+)^T (s_1 \mathbf{B}_\Theta^{\alpha-} + s_2 \mathbf{B}_\Theta^{\alpha+}) d\Gamma \check{\Theta} \\ & - \int_{\Gamma_s} k \frac{w}{2} (s_2 \Phi_\Theta^- + s_1 \Phi_\Theta^+)^T (s_2 \mathbf{B}_\Theta^{\alpha-} + s_1 \mathbf{B}_\Theta^{\alpha+}) d\Gamma \check{\Theta}, \end{aligned} \quad (45)$$

where \mathbf{B}_Θ^α is defined as $\mathbf{B}_\Theta^\alpha = \frac{\partial \Phi_\Theta}{\partial \alpha}$.

The smoothed heat flux $\mathbf{q}^* = \Phi_q \check{\mathbf{q}}^*$ obtained from Eq. (38) or Eq. (43) is then used for measuring the error for particular finite element cells, i.e.:

$$\epsilon_{zz}^e = \frac{1}{|\Omega^e|} \int_{\Omega^e} (\Phi_q \check{\mathbf{q}}^* + k \mathbf{B}_\Theta \check{\Theta})^T (\Phi_q \check{\mathbf{q}}^* + k \mathbf{B}_\Theta \check{\Theta}) d\Omega, \quad (46)$$

where Ω^e is the volume of the e -th finite element cell, ϵ_{zz}^e is the error measure for e -th finite element cell. It should be noted that in Eq. (32) the error measure is for the whole domain and is constructed in order to find the smoothed flux \mathbf{q}^* . Then the element error measure can be directly calculated from Eq. (46).

7. THE hp -TYPE MESH REFINEMENT

Two types of finite elements are used in the approach presented in this paper: the regular finite elements and the skeleton finite elements. The regular finite elements are typical as standard finite elements shape functions are used for approximation in these elements. The skeleton finite elements are not typical finite elements since they are very thin and the approximation is based on the values on both sides of the skeleton segment. The skeleton finite elements can quite easily join neighbouring elements with a different approximation order, e.g., the three-node finite element with ten-node finite element, like in Fig. 5. It is also possible to use this method to join non-conforming finite element cells, also with different number of nodes. This is illustrated in Fig. 6,

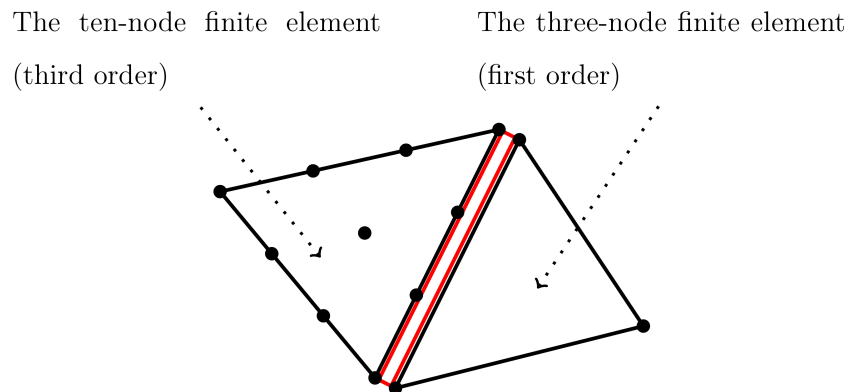


Fig. 5. The configuration of two neighbouring finite element cells with different approximation order.

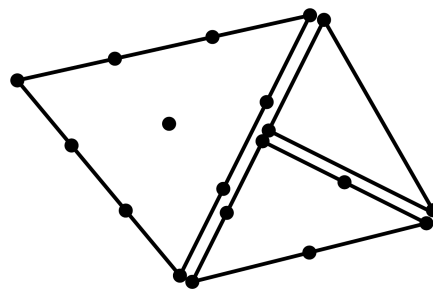


Fig. 6. The configuration of three neighbouring non-conforming finite element cells with different numbers of nodes.

where three neighbouring non-conforming finite elements with different number of nodes are joined by skeleton finite elements.

This paper is concerned with the refinement of h -type or p -type as well as the combined hp -type refinement. By using the skeleton finite elements, all types of refinements are easy to perform. In a situation when we want to refine a certain single element, the refinement procedure can be reduced to this particular element.

The refinement procedure is based on the ZZ error measure. For each element the error in Eq. (46) is calculated and then this element can be refined. The refinement procedure is as follows:

1. Prepare the finite element mesh, each element is of the first order.
2. Find the approximated solution for the mesh.
3. Find the smoothed heat flux \mathbf{q}^* .
4. Set two error limits β_1 and β_2 where $\beta_1 < \beta_2$.
5. Compute ϵ_{zz}^e for each element.
6. Each element is divided into two elements when $\epsilon_{zz}^e > \beta_1$.
7. When $\epsilon_{zz}^e > \beta_2$, the elements are additionally p refined (the order of the elements is increased).
8. Afterwards, the problem is solved on the refined mesh and subsequently the points 1–8 are repeated.
9. The procedure stops when no element in the mesh is refined.

In the examples presented in Subsec. 9.1, a two-dimensional problem is presented. For those problems, the triangular meshes are used, which are refined using the procedure described in

this section. For p refinement, the following sequences of triangular elements are used: 1st order (3 nodes), 2nd order (6 nodes), 3rd order (10 nodes), 4th order (15 nodes), 5th order (21 nodes), 6th order (28 nodes). 7th order (36 nodes). The high-order finite elements are constructed using the procedure presented in [2]. In a case when an element reaches 7th order of approximation the element can be only h -type refined.

The hp refinement technique presented in this paper is easy to implement and it is not restrictive in the sense of element division or raising the element order. The refinement of one element does not influence the neighbouring elements. The usage of special finite elements, i.e., skeleton finite elements, gives a great opportunity for a combined hp refinement. This technique gives a great flexibility in the mesh refinement, which can be easily adjusted to fit particular requirements.

8. EVALUATION OF THE SKELETON WIDTH

In order to obtain correct results from the IDG method, the skeleton width w has to be properly assessed. Its value depends strictly on the mesh density. A short analysis concerning the skeleton width is presented in this section, which finally results in a practical method of w assessment. Similar approach is presented in [30] where the interface region is applied for coupling two computer methods. In this work the procedure is adjusted to the skeleton width assessment.

In the IDG method, the volume of the finite element mesh consists of the volume of all finite elements $|\Omega_s|$ and the volume of the mesh skeleton $|\Omega_E|$. It is required that the skeleton volume should be much smaller in relation to the volume of the regular finite elements. This can be expressed as

$$\frac{|\Omega_s|}{|\Omega_E|} = \epsilon(h), \quad (47)$$

where h is the characteristic length of finite element in the mesh, and ϵ is a small value which depends on the element size. After the analogous analysis presented in [30] the value of the skeleton width can be expressed as

$$w = C \cdot h \cdot \left(\arctan \left(\frac{h}{\rho} - 1 \right) + \frac{\pi}{2} \right), \quad (48)$$

where C and ρ are constants independent of the mesh density. These constants need to be set for the considered problem. In this work they are set as $C = 1 \cdot 10^{-7}$ and $\rho = 1 \cdot 10^{-1}$.

9. EXAMPLES

9.1. Benchmark example

The presented approach is illustrated in this section with a two-dimensional exponential example. In the considered example, a square domain $[-1, 1] \times [-1, 1]$ is taken into account, in which the exact solution of an elliptic problem is given as

$$\Theta(x, y) = \exp(-5 \cdot (x - y)^2 - 5x^2). \quad (49)$$

The function, shown in Fig. 7, has large gradients and this is why it is suitable for numerical tests.

The function is used to construct the boundary problem in the form

$$-\Delta\Theta = f(x, y), \quad (50)$$

where the Dirichlet boundary conditions are applied on all the outer boundaries, and the values are taken from the function in Eq. (49). The problem defined in (50) can be seen as a heat transport

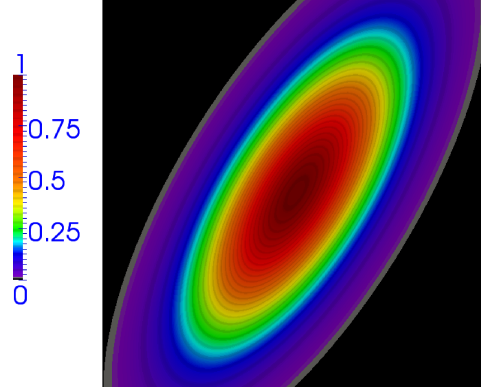


Fig. 7. The exact solution of the considered example $\Theta(x, y) = \exp(-5 \cdot (x - y)^2 - 5x^2)$.

problem, where the thermal conductivity is $k = 1$ and the heat source r is given by the function $f(x, y)$, which is defined as

$$f(x, y) = (-50x^2 + 60xy - 20y^2 + 3) \cdot \exp(-5 \cdot (x - y)^2 - 5x^2). \quad (51)$$

The considered example is solved using the IDG method for various finite element meshes and of various order of finite elements. The results obtained from the IDG method are compared with the exact solution in Eq. (49).

In our benchmark example, two kinds of errors are considered: the temperature error ϵ_Θ and flux error ϵ_q which are defined as follows:

$$\epsilon_\Theta = |\Theta - \Theta^h|, \quad \epsilon_q = \sqrt{(\mathbf{q} - \mathbf{q}^h)^\top (\mathbf{q} - \mathbf{q}^h)}, \quad (52)$$

where Θ^h and \mathbf{q}^h are the approximate temperature and heat flux, respectively.

Two kinds of global errors in L_2 norm and H_1 semi-norm, i.e.,

$$\|\epsilon_\Theta\|_2 = \sqrt{\int_{\Omega} (\epsilon_\Theta)^2 d\Omega}, \quad |\epsilon_\Theta|_1 = \sqrt{\int_{\Omega} (\epsilon_q)^2 d\Omega} \quad (53)$$

are used in the following analysis. In some cases, the global effectivity index is also traced, which is defined as

$$I_\epsilon = \frac{\sqrt{\int_{\Omega} (\epsilon_q^*)^2 d\Omega}}{\sqrt{\int_{\Omega} (\epsilon_q)^2 d\Omega}}, \quad (54)$$

where ϵ_q^* is defined as

$$\epsilon_q^* = \sqrt{(\mathbf{q}^* - \mathbf{q}^h)^\top (\mathbf{q}^* - \mathbf{q}^h)}. \quad (55)$$

The analysed problem has been solved using uniform meshes (i.e., the size of all finite elements in a mesh is about the same) but with various densities so that convergence of the IDG method could be verified. The convergence test has been done for finite elements of the first order up to sixth order. The results are presented in Fig. 8, where the errors are shown in relation to the element size. The results show the well-known tendency that the finite elements of higher order not only give more accurate results but also a higher convergence rate.

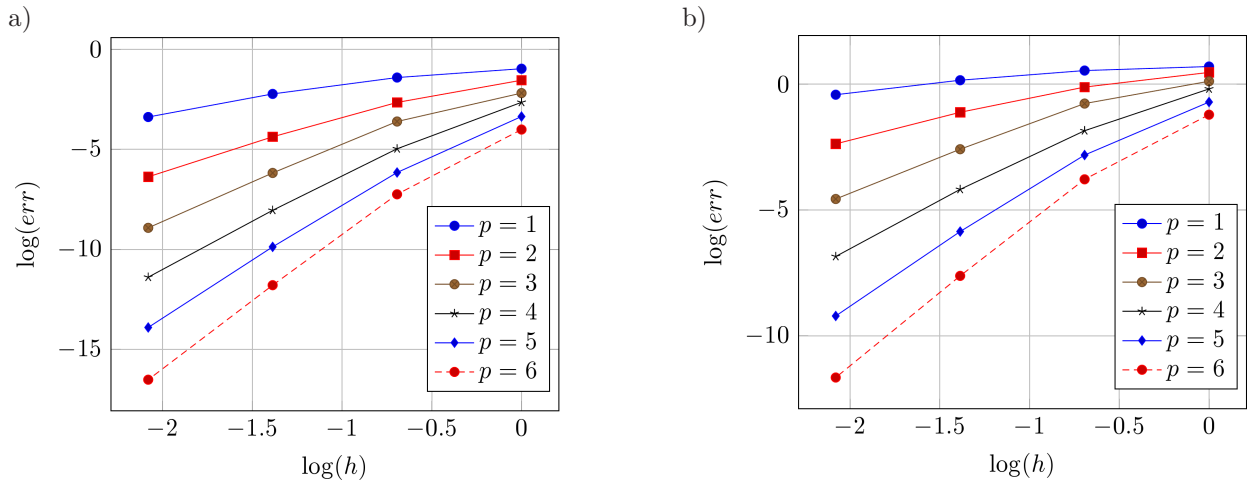


Fig. 8. Convergence of the IDG method for finite elements of the 1st up to 6th order:
 a) convergence in L_2 norm, b) convergence in H_1 semi-norm.

In the next step, the problem in Eq. (50) has been solved on the non-conforming rough mesh (21 cells) but with elements of the 1st to 6th order. The results are presented in Fig. 9, and they show that the IDG method gives results that are continuous, even for non-conforming meshes and for elements with various order.

Subsequently, three cases are presented illustrating the mesh non-conformity. Figure 10 presents the results obtained where the finite element mesh is regular and conforming. In this case, the first-order finite elements are used (i.e., three degrees of freedom – dofs). The results are in fact the same as the results obtained by the standard FEM. In the second case, the non-conforming mesh is used. The mesh and the results obtained for the mesh are presented in Fig. 11. In this case, all finite elements are of the first order (3 dofs). In spite of the fact that the finite elements are non-conforming, the results are continuous for the whole domain. This shows that in the IDG method the mesh conformity is not required. In the third case, the non-conforming mesh is used and the finite elements in the mesh are of various orders. Figure 12a presents the mesh for the third case with the number of dofs for finite elements. In this case, the finite elements with 3, 6 and 28 dofs are used and the elements of the first order (3 dofs) are located next to the 6-th order finite elements (28 dofs). The results presented in Fig. 12b are continuous, even though two first order finite elements are surrounded by 6-th order finite elements. This means that in the IDG method, the h -type and p -type refinements can be done quite easily. The arbitrary element in the mesh can be divided or its order can be raised without any change in the neighbouring elements.

The same example as the one defined in Eqs. (49)–(51) is used for illustrating the h -type and hp -type refinements. The refinement procedure outlined in Sec. 7 is applied here for h and, subsequently, for hp refinement. In the refinement procedure, the error measure for each element is calculated accordingly to Eq. (46). The h -type refinement procedure with the uniform order p for finite elements is assumed. The calculations have been performed for $p = 1, 2, 3$. In each case, the initial mesh consisted of 32-element triangular mesh and 12 refinement steps have been performed. The β_1 parameter has been set to $5 \cdot 10^{-5}$, $1 \cdot 10^{-7}$ and $1 \cdot 10^{-10}$ for $p = 1, 2, 3$, respectively. Finally, the h -type refinement was compared to hp -type refinement. In the hp -type refinement the parameters β_1 and β_2 were set to $1 \cdot 10^{-12}$ and $1 \cdot 10^{-10}$. In this case, the same initial mesh has been used and only six refinement steps were sufficient to get the results of high accuracy. The results are presented in the form of solution convergence in relation to the number of degrees of freedom ($\#\text{dof}$), Fig. 13. Figure 14 shows the effectivity index for h refinement with $p = 3$ and for hp refinement. The meshes and errors maps are presented in Figs. 15–17 after 7th and 12th steps for h -type refinement. For the hp -type refinement, the final mesh with various values of p and error map is shown in Fig. 18.

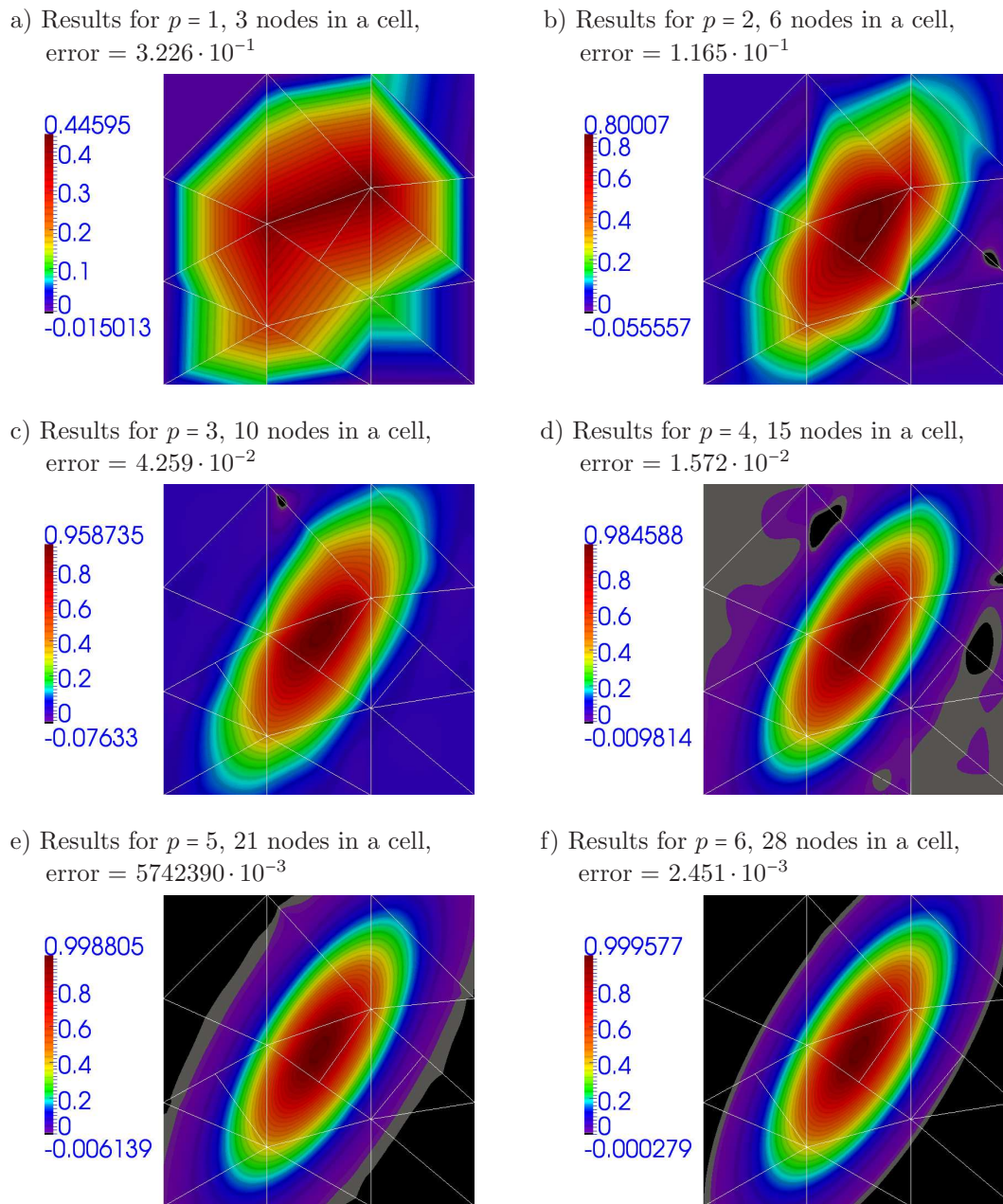


Fig. 9. The results of the IDG method for various orders p on a non-conforming mesh with 21 cells.

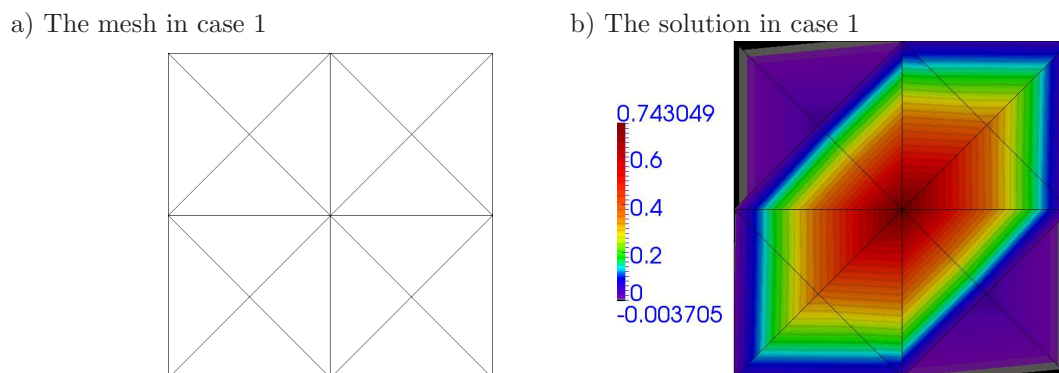
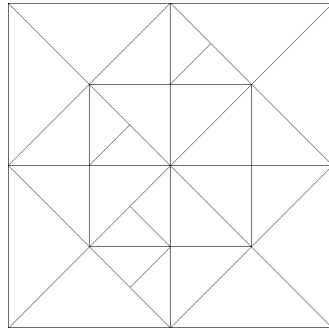


Fig. 10. The mesh and solution for case 1. The mesh is conforming and finite elements are of the first order.

a) The mesh in case 2



b) The solution in case 2

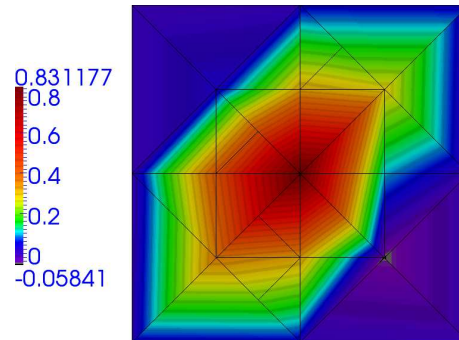
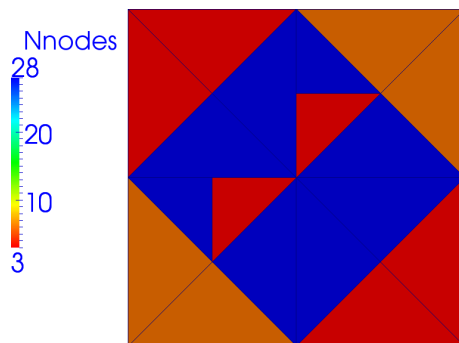


Fig. 11. The mesh and solution for case 2. The mesh is non-conforming and finite elements are of the first order.

a) The mesh in case 3.

The colors in the elements represent the number of dofs (red – 3 dofs, orange – 6 dofs, blue – 28 dofs)



b) The IDGM solution in case 3

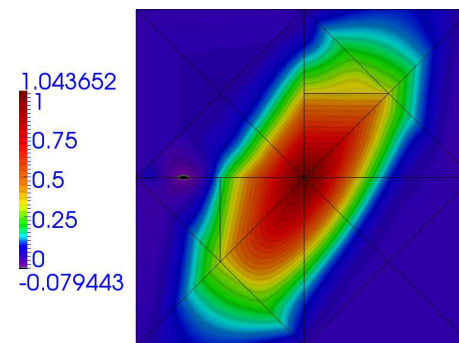
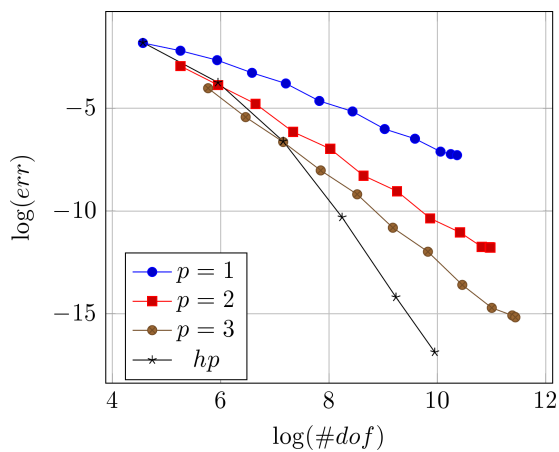


Fig. 12. The mesh and solution for case 3. The mesh is non-conforming and finite elements are of various orders.

a)



b)

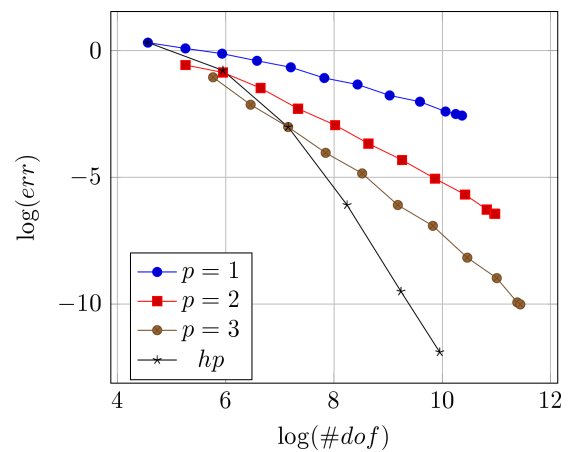


Fig. 13. Solution convergence in h -type refinement for $p = 1, 2, 3$ and hp -type refinement: a) convergence in L_2 norm, b) convergence in H_1 semi-norm.

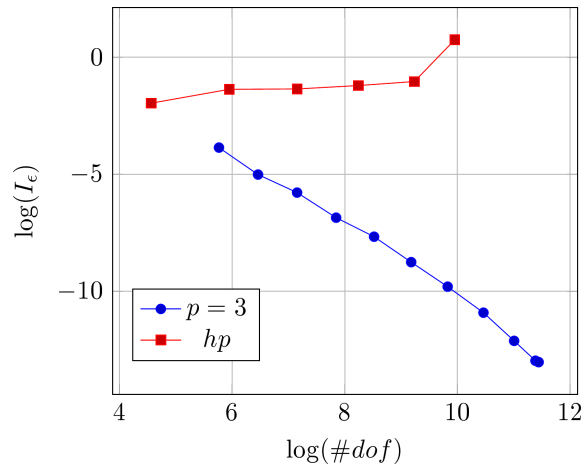


Fig. 14. Effectivity index for h -type refinement with $p = 3$ and hp refinement.

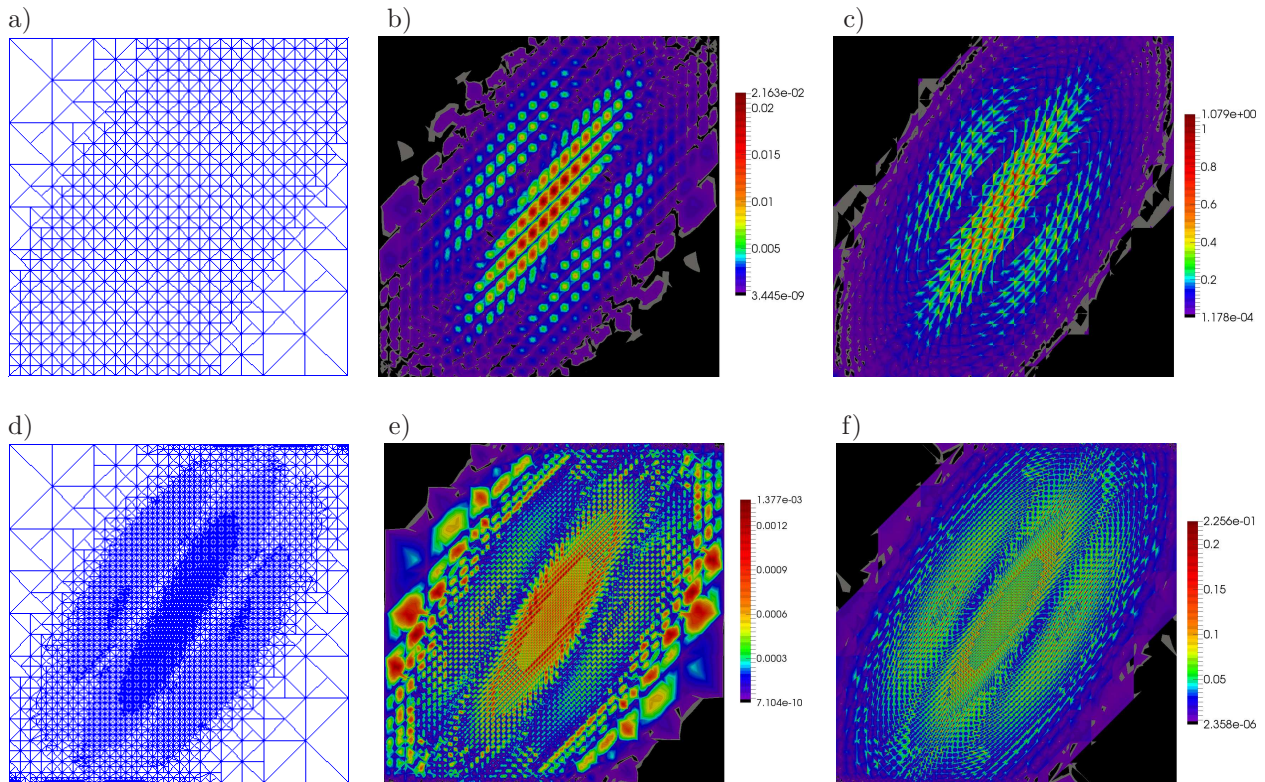


Fig. 15. h -Type refinement for $p = 1$. The mesh, ϵ_Θ error map and ϵ_q error map after 11th step: (a), (b), (c) and after 16th step: (d), (e), (f).

From the presented results it can be noticed that the h -type mesh refinement procedure for various p can follow the places with higher errors. The mesh is refined in such a way so that the error distribution is more or less uniformly distributed in the whole domain. However, for higher order elements the convergence rate is higher. Similar effect is obtained for hp -type refinement. However, in this case, the approximate solution convergence is the fastest. For hp -type refinement the relatively small $\#dofs$ is needed for high-quality solution. For example, 21 thousand $\#dofs$ was enough for hp -type refinement to reach error level of $4 \cdot 10^{-8}$ and in h -type refinement and $p = 3$, 93 thousand $\#dofs$ is used to obtain error level of $2 \cdot 10^{-7}$.

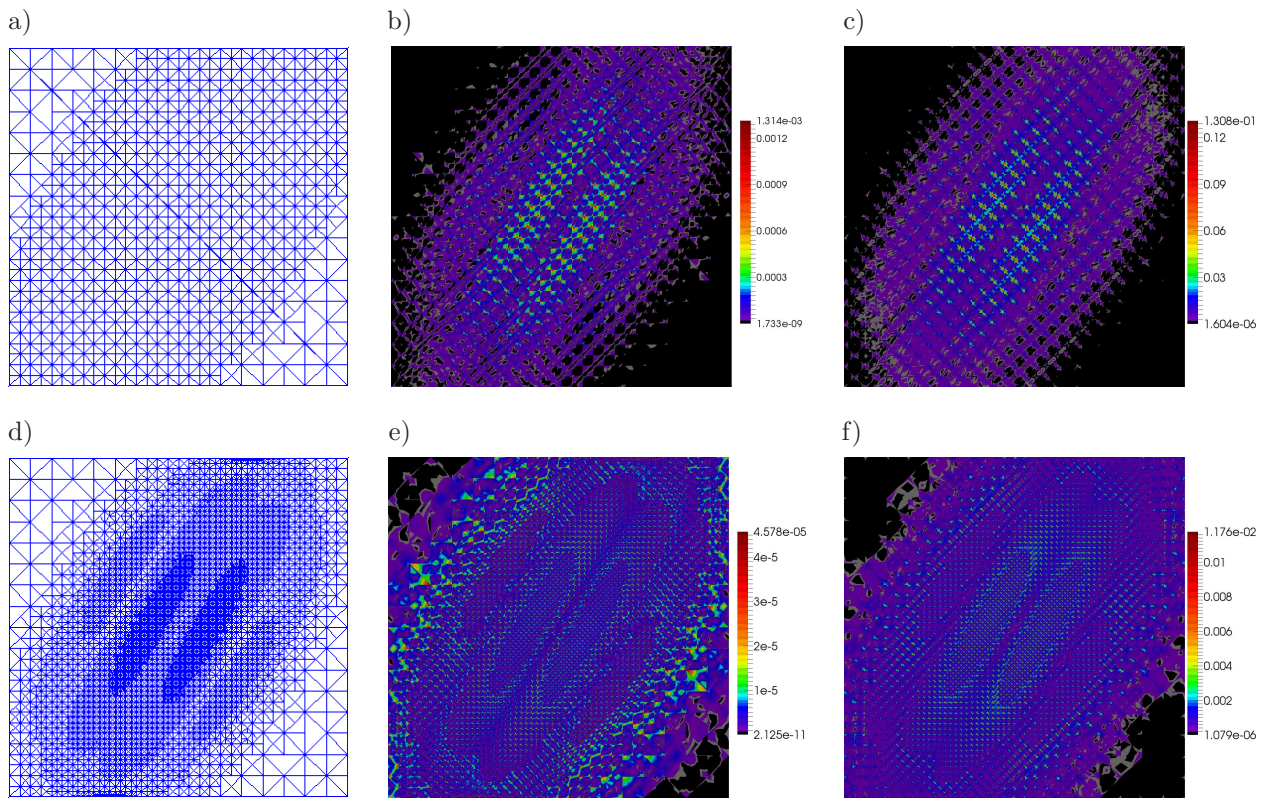


Fig. 16. h -Type refinement for $p = 2$. The mesh, ϵ_{Θ} error map and ϵ_q error map after 11th step: (a), (b), (c) and after 16th step: (d), (e), (f).

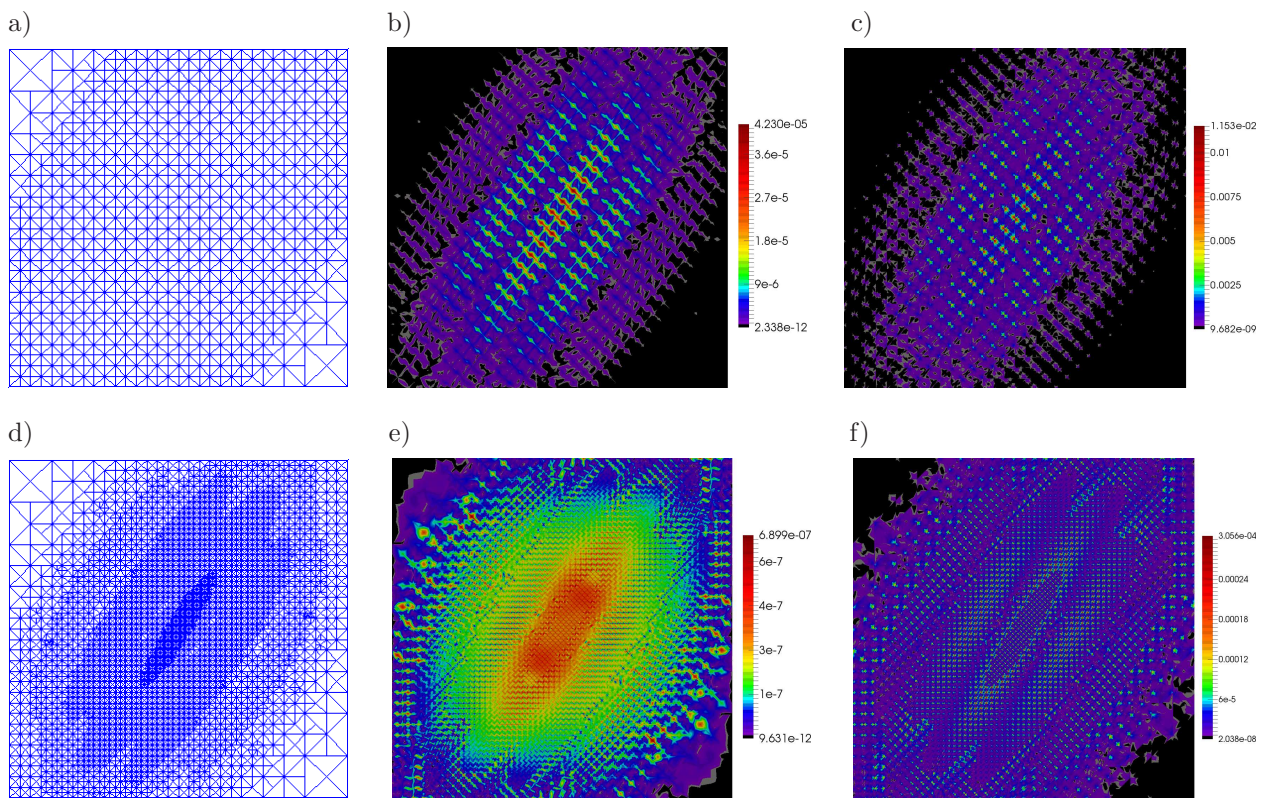


Fig. 17. h -Type refinement for $p = 3$. The mesh, ϵ_{Θ} error map and ϵ_q error map after 11th step: (a), (b), (c) and after 16th step: (d), (e), (f).

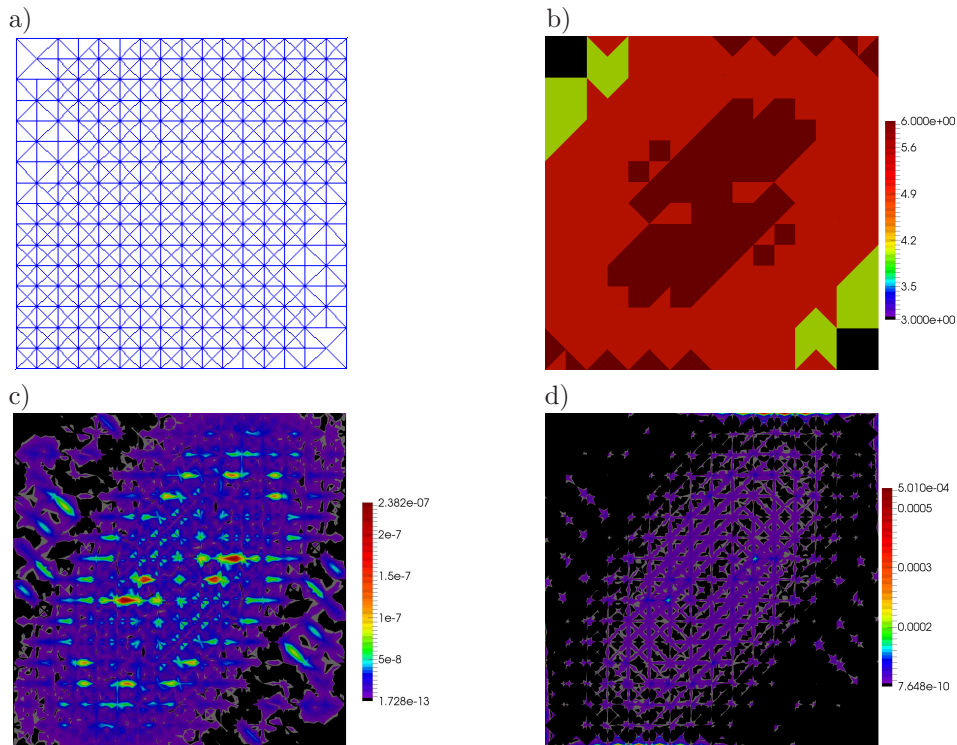


Fig. 18. The results of hp -type refinement after the final step: a) mesh, b) p -order map, c) ϵ_Θ error map, d) ϵ_q error map.

9.2. Domain with rectangular hole example

This example illustrates the heat flow through the domain with a hole. Figure 19 shows the domain with the boundary conditions and the reference solution of the problem. The reference solution has

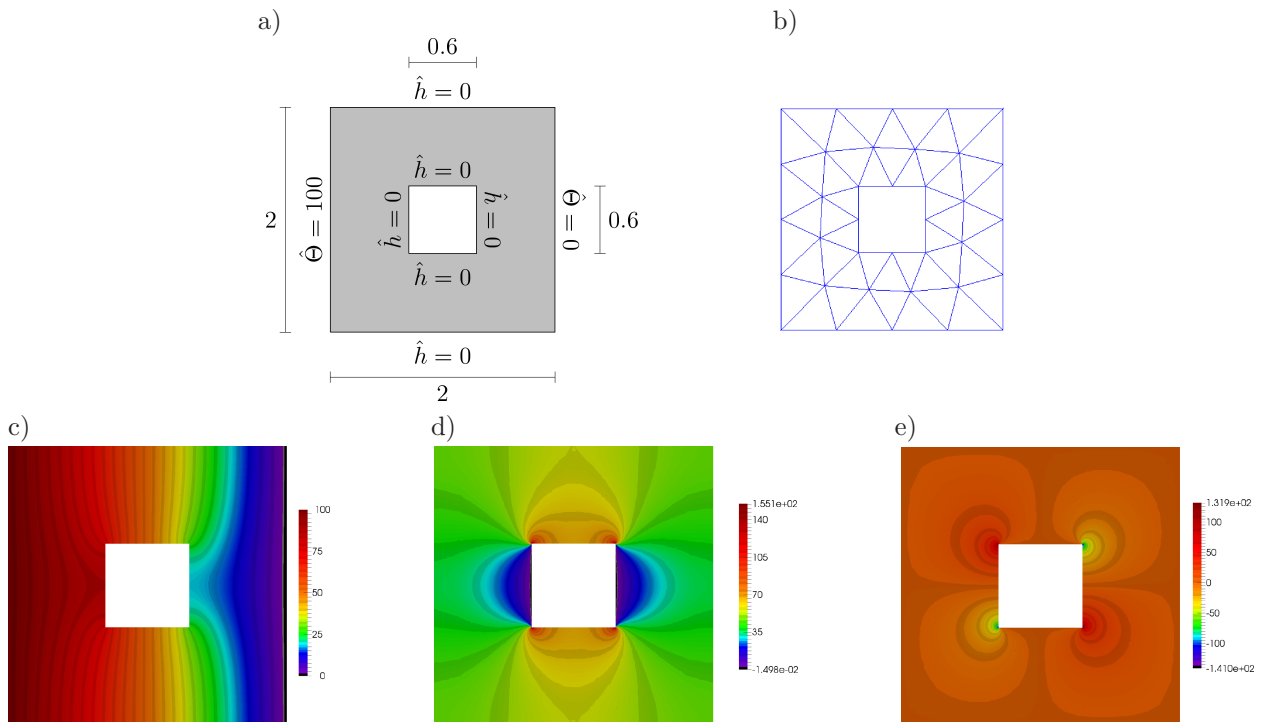


Fig. 19. Domain with a hole for heat transfer example: a) domain with boundary conditions, b) initial mesh with 48 finite elements and 144 #dofs and reference solution: c) temperature Θ , d) heat flux q_x , e) heat flux q_y .

been obtained on a very dense mesh with third degree finite elements using a standard FEM. The heat flux on the vertices goes to infinity, so the upper and lower boundaries for q_x and q_y have

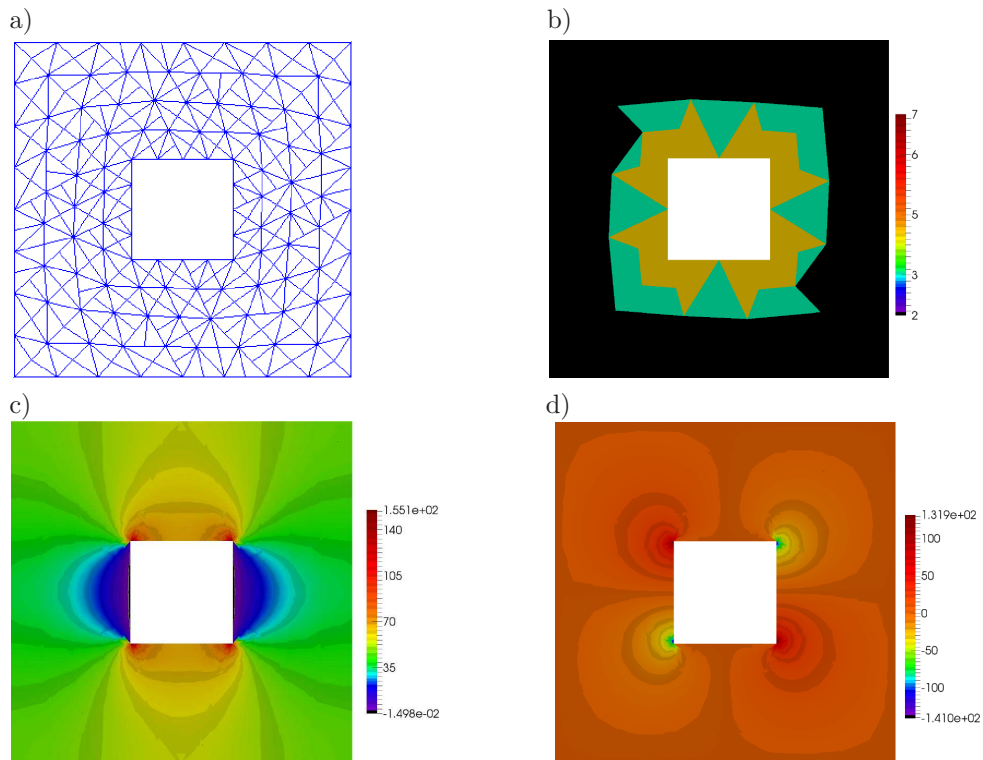


Fig. 20. The results of hp -type refinement after the 4th step: a) mesh with 384 finite elements and 3312 #dofs, b) p -order map, c) heat flux in x direction, d) heat flux in y direction.

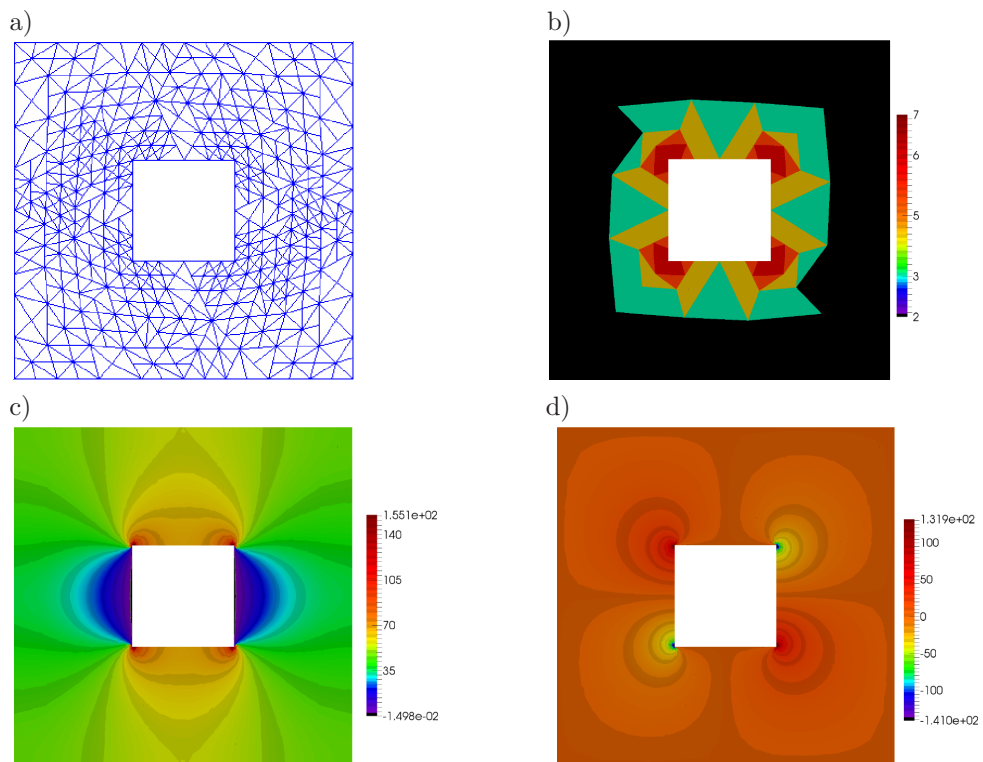


Fig. 21. The results of hp -type refinement after the 6th step: a) mesh with 848 finite elements and 8568 #dofs, b) p -order map, c) heat flux in x direction, d) heat flux in y direction.

been set on the figures with heat fluxes. For the sake of clarity, all the values in this example are dimensionless and the conductivity parameter k is set to one.

In this example, the heat flux concentration is observed on the inside hole vertices. So the mesh refinement should be concentrated around these vertices. In this example, 14 hp -type refinement steps were performed and the parameters β_1 and β_2 were set to $1 \cdot 10^{-3}$ and $1 \cdot 10^{-1}$ respectively. The results after 4th, 6th and 14th steps are presented in Figs. 20–22, respectively.

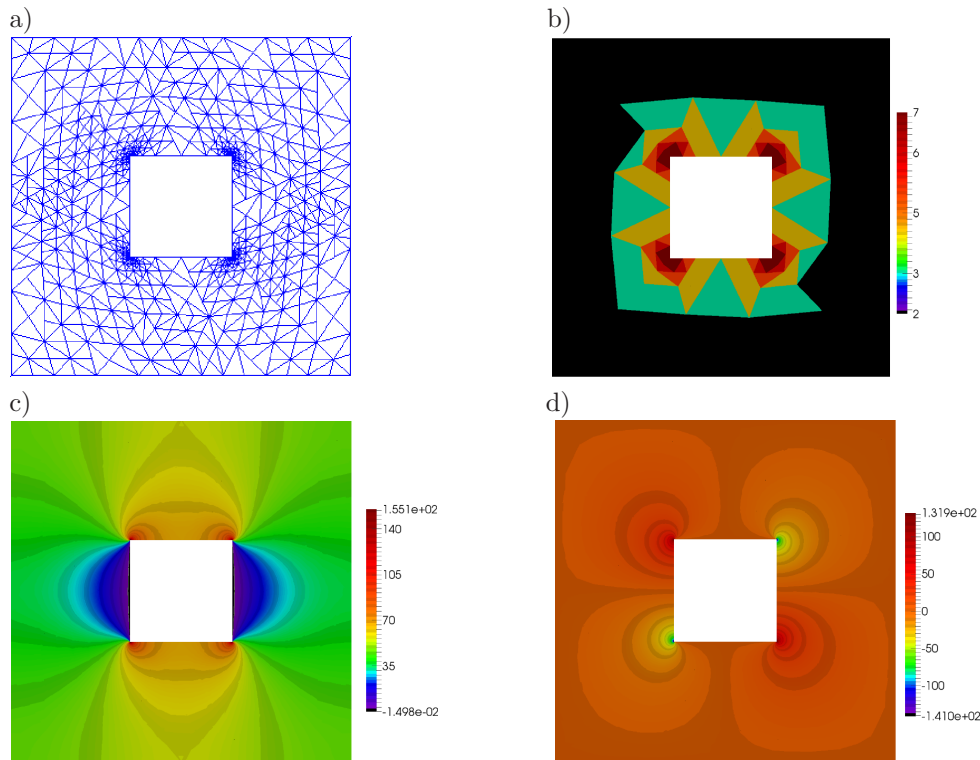


Fig. 22. The results of hp -type refinement after the 14th step: a) mesh with 1424 finite elements and 28752 #dofs, b) p -order map, c) heat flux in x direction, d) heat flux in y direction.

It can be noticed that the mesh is refined just around the hole vertices, thus in the places with heat flux concentrations. This means that the refinement procedure can find the places with higher errors and reduce the error levels.

10. CONCLUSIONS

This paper presents the so-called IDG method with its applications to the elliptic problem of stationary heat transport. The IDG method is quite similar to SDG method that is well known from the literature. However, the IDG method results in different equations in comparison to SDG and it is quite simple to adapt the ZZ estimator to the IDG approach. The core idea of the IDG formulation is that the mesh skeleton has a non-zero thickness and is discretized by special, very thin, finite elements. Those skeleton finite elements play a role of interfaces between the regular finite elements. As a result, the considered domain volume is divided into the regular finite elements and the special skeleton finite elements between them. Due to a small thickness of the skeleton volume, the integrals over the volume are expressed by integrals along the skeleton surface. Next, all the quantities in the skeleton volume are substituted by finite difference relations or mid-values over the skeleton thickness.

In the IDG method, the mesh refinement of h - or p -type, or their combination, is quite simple. In the refinement of the finite element mesh, the neighbouring elements do not have to be geometrically

conforming. In addition, there is no problem, if the neighbouring elements are of different orders, e.g., first and seventh order or so on. The mesh refinement procedure described in this paper is based on the ZZ error estimation. The ZZ procedure is adopted for the IDG method. In consequence, a simple and effective algorithm for error estimation, based on element error indicators, is obtained.

It is important to assess the skeleton width and that the width should depend on the size of finite elements. The technique presented in this paper helps to assess effectively the skeleton thickness for calculations. The approach presented in this paper can be directly extended to other kinds of problems, for example, a diffusion-dominated problem or coupled problems. This will be the subject of our further research.

REFERENCES

- [1] M Ainsworth. A posteriori error estimation for discontinuous Galerkin finite element approximation. *SIAM Journal on Numerical Analysis*, **45**(4): 1777–1798, 2007.
- [2] J.H. Argyris, I. Fried, D.W. Scharpf. The TUBA family of plate elements for the matrix displacement method. *The Aeronautical Journal*, **72**(692): 701–709, 1968.
- [3] D.N. Arnold, F. Brezzi, B. Cockburn, L.D. Marini. Unified analysis of discontinuous Galerkin methods for elliptic problems. *SIAM J. Numer. Anal.*, **39**(5): 1749–1779, May 2001.
- [4] G. Billet, J. Ryan. A Runge-Kutta discontinuous Galerkin approach to solve reactive flows: The hyperbolic operator. *Journal of Computational Physics*, **230**(4): 1064–1083, 2011.
- [5] T. Bui-Thanh, O. Ghattas. Analysis of an hp -nonconforming discontinuous Galerkin spectral element method for wave propagation. *SIAM Journal on Numerical Analysis*, **50**(3): 1801–1826, 2012.
- [6] N.K. Burgess, D.J. Mavriplis. hp -Adaptive discontinuous Galerkin solver for the Navier-Stokes equations. *American Institute of Aeronautics and Astronautics*, **50**(12): 2682–2692, 2012.
- [7] E. Burman, B. Stamm. Bubble stabilized discontinuous Galerkin methods on conforming and non-conforming meshes. *Calcolo*, **48**(2): 189–209, 2011.
- [8] U.H. Çalık-Karaköse, H. Askes. A recovery-type a posteriori error estimator for gradient elasticity. *Computers & Structures*, **154**: 204–209, 2015.
- [9] Y Chen, J. Huang, Y Huang, Y Xu. On the local discontinuous Galerkin method for linear elasticity. *Mathematical Problems in Engineering*, **2010**: 20 pp., 2010.
- [10] B. Cockburn, C-W. Shu. The local discontinuous Galerkin method for time-dependent convection-diffusion systems. *SIAM Journal on Numerical Analysis*, **35**(6): 2440–2463, 1998.
- [11] B. Cockburn, C-W. Shu. TVB Runge-Kutta local projection discontinuous Galerkin finite element method for conservation laws. II. General framework. *Mathematics of Computation*, **52**(186): 411–435, 1989.
- [12] B. Cockburn, S. Hou, C-W. Shu. The Runge-Kutta local projection discontinuous Galerkin finite element method for conservation laws. IV. The multidimensional case. *Mathematics of Computation*, **54**: 545–581, 1990.
- [13] B. Cockburn, S. Lin, C-W. Shu. TVB Runge-Kutta local projection discontinuous Galerkin finite element method for conservation laws III: One-dimensional systems. *Journal of Computational Physics*, **84**(1): 90–113, September 1989.
- [14] E. Creusé, S. Nicaise. A posteriori error estimator based on gradient recovery by averaging for discontinuous Galerkin methods. *Journal of Computational and Applied Mathematics*, **234**(10): 2903–2915, 2010.
- [15] C. Dawson, S. Sun, M.F. Wheeler. Compatible algorithms for coupled flow and transport. *Computer Methods in Applied Mechanics and Engineering*, **193**(23–26): 2565–2580, 2004.
- [16] L. Demkowicz, J.T. Oden, W. Rachowicz, O. Hardy. Toward a universal h-p adaptive finite element strategy. Part 1. Constrained approximation and data structure. *Computer Methods in Applied Mechanics and Engineering*, **77**(1): 79–112, 1989.
- [17] L.F. Demkowicz, K. Banas, J. Kucwaj, W. Rachowicz. 2D hp adaptive package. Technical Report SAM Report 4/1992, Section of Applied Mathematics, Cracow University of Technology, September 1992.
- [18] G. Engel, K. Garikipati, T.J.R. Hughes, M.G. Larson, L. Mazzei, R.L. Taylor. Continuous/discontinuous finite element approximations of fourth-order elliptic problems in structural and continuum mechanics with applications to thin beams and plates, and strain gradient elasticity. *Computer Methods in Applied Mechanics and Engineering*, **191**(34): 3669–3750, 2002.
- [19] Y. Epshteyn, B. Rivière. Analysis of discontinuous Galerkin methods for incompressible two-phase flow. *Journal of Computational and Applied Mathematics*, **225**(2): 487–509, 2009.
- [20] A. Ern, J. Proft. A posteriori discontinuous Galerkin error estimates for transient convection-diffusion equations. *Applied Mathematics Letters*, **18**(7): 833–841, 2005.
- [21] H. Fahs, S. Lanteri. A high-order non-conforming discontinuous Galerkin method for time-domain electromagnetics. *Journal of Computational and Applied Mathematics*, **234**(4): 1088–1096, 2010. Proceedings of the Thirteenth

- International Congress on Computational and Applied Mathematics (ICCAM-2008), Ghent, Belgium, 7–11 July, 2008.
- [22] P.E. Farrell, S. Micheletti, S. Perotto. An anisotropic Zienkiewicz-Zhu-type error estimator for 3D applications. *International Journal for Numerical Methods in Engineering*, **85**(6): 671–692, 2011.
- [23] D. Fournier, R. Herbin, R. Tellier. Discontinuous Galerkin discretization and *hp*-refinement for the resolution of the neutron transport equation. *SIAM Journal on Scientific Computing*, **35**(2): A936–A956, 2013.
- [24] G. Gassner, M. Staudenmaier, F. Hindenlang, M. Atak, C.-D. Munz. A space-time adaptive discontinuous Galerkin scheme. *Computers & Fluids*, **117**: 247–261, 2015.
- [25] E. Georgoulis, E. Hall, P. Houston. Discontinuous Galerkin methods for advection-diffusion-reaction problems on anisotropically refined meshes. *SIAM Journal on Scientific Computing*, **30**(1): 246–271, 2008.
- [26] S. Giani, D. Schötzau, L. Zhu. An a-posteriori error estimate for *hp*-adaptive DG methods for convection-diffusion problems on anisotropically refined meshes. *Computers & Mathematics with Applications*, High-order Finite Element Approximation for Partial Differential Equations, **67**(4): 869–887, 2014.
- [27] G. Haikal, K.D. Hjelmstad. An enriched discontinuous Galerkin formulation for the coupling of non-conforming meshes. *Finite Elements in Analysis and Design*, The Twenty-First Annual Robert J. Melosh Competition, **46**(6): 496–503, 2010.
- [28] P. Hansbo, M.G. Larson. Discontinuous Galerkin methods for incompressible and nearly incompressible elasticity by Nitsche’s method. *Computer Methods in Applied Mechanics and Engineering*, **191**(17–18): 1895–1908, 2002.
- [29] P. Houston, B. Senior, E. Süli. *hp*-Discontinuous Galerkin finite element methods for hyperbolic problems: error analysis and adaptivity. *International Journal for Numerical Methods in Fluids*, **40**(1–2): 153–169, 2002.
- [30] J. Jaśkowiec, S. Milewski. The effective interface approach for coupling of the FE and meshless FD methods and applying essential boundary conditions. *Computers & Mathematics with Applications*, **70**(5): 962–979, 2015.
- [31] J. Jaśkowiec, P. Pluciński, J. Pamin. Thermo-mechanical XFEM-type modeling of laminated structure with thin inner layer. *Engineering Structures*, 100:511–521, 2015.
- [32] L. Ji, Y. Xu. Optimal error estimates of the local discontinuous Galerkin method for surface diffusion of graphs on Cartesian meshes. *J. Sci. Comput.*, **51**(1): 1–27, April 2012.
- [33] B. Karasözen, M. Uzunca, M. Manguoğlu. Adaptive discontinuous Galerkin methods for nonlinear diffusion-convection-reaction equations. [In:] A. Abdulle, S. Deparis, D. Kressner, F. Nobile, M. Picasso [Eds.], *Numerical Mathematics and Advanced Applications – ENUMATH 2013*, vol. 103 of *Lecture Notes in Computational Science and Engineering*, pp. 85–93. Springer International Publishing, 2015.
- [34] H.H. Kim, E.T. Chung, C.-Y. Lam. Mortar formulation for a class of staggered discontinuous Galerkin methods. *Computers & Mathematics with Applications*, **71**(8): 1568–1585, 2016.
- [35] S. Micheletti, S. Perotto. Reliability and efficiency of an anisotropic Zienkiewicz-Zhu error estimator. *Computer Methods in Applied Mechanics and Engineering*, **195**(9–12): 799–835, 2006.
- [36] D.A. Di Pietro, S. Nicaise. A locking-free discontinuous Galerkin method for linear elasticity in locally nearly incompressible heterogeneous media. *Applied Numerical Mathematics*, **63**: 105–116, 2013.
- [37] W.H. Reed, T.R. Hill. Triangular mesh methods for the neutron transport equation. Technical Report LA-UR-73-479, Los Alamos Scientific Laboratory, Oct 1973.
- [38] B. Rivière. *Discontinuous Galerkin Methods for Solving Elliptic and Parabolic Equations: Theory and Implementation*. Frontiers in Applied Mathematics. Society for Industrial and Applied Mathematics, 2008.
- [39] B. Rivière, M. Wheeler, V. Girault. A priori error estimates for finite element methods based on discontinuous approximation spaces for elliptic problems. *SIAM Journal on Numerical Analysis*, **39**(3): 902–931, 2001.
- [40] B. Rivière, M.F. Wheeler, K. Banaś. Part II. Discontinuous Galerkin method applied to a single phase flow in porous media. *Computational Geosciences*, **4**(4): 337–349, 2000.
- [41] R. Schneider, Y. Xu, A. Zhou. An analysis of discontinuous Galerkin methods for elliptic problems. *Advances in Computational Mathematics*, **25**(1–3): 259–286, 2006.
- [42] Y. Shen, A. Lew. Stability and convergence proofs for a discontinuous-Galerkin-based extended finite element method for fracture mechanics. *Computer Methods in Applied Mechanics and Engineering*, **199**(37–40): 2360–2382, 2010.
- [43] Y. Shen, A.J. Lew. A locking-free and optimally convergent discontinuous-Galerkin-based extended finite element method for cracked nearly incompressible solids. *Computer Methods in Applied Mechanics and Engineering*, **273**: 119–142, 2014.
- [44] L. Song, Z. Zhang. Superconvergence property of an over-penalized discontinuous Galerkin finite element gradient recovery method. *Journal of Computational Physics*, **299**: 1004–1020, 2015.
- [45] F. Stan. Discontinuous Galerkin method for interface crack propagation. *International Journal of Material Forming*, **1**(1): 1127–1130, 2008.
- [46] B.A. Szabó, I. Babuška. *Finite Element Analysis*. John Wiley & Sons Inc., New York, 1991.
- [47] M. Uzunca, B. Karasözen, M. Manguoğlu. Adaptive discontinuous Galerkin methods for non-linear diffusion-convection-reaction equations. *Computers & Chemical Engineering*, **68**: 24–37, 2014.
- [48] G.N. Wells, K. Garikipati, L. Molari. A discontinuous Galerkin formulation for a strain gradient-dependent damage model. *Computer Methods in Applied Mechanics and Engineering*, **193**(33–35): 3633–3645, 2004.

- [49] M. Wheeler. An elliptic collocation-finite element method with interior penalties. *SIAM Journal on Numerical Analysis*, **15**(1): 152–161, 1978.
- [50] G. Zboinski. Application of the three-dimensional triangular-prism hpq adaptive finite element to plate and shell analysis. *Computers & Structures*, **65**(4): 497–514, 1997.
- [51] G. Zboński. *Hierarchical Modeling and Finite Element Approximation for Adaptive Analysis of Complex Structures* [in Polish: *Modelowanie hierarchiczne i metoda elementów skończonych do adaptacyjnej analizy struktur złożonych*]. DSc Thesis, 520/1479/2001. Institute of Fluid Flow Machinery, Gdańsk, 2001.
- [52] Q. Zhang, C-W. Shu. Stability analysis and a priori error estimates of the third order explicit Runge-Kutta discontinuous Galerkin method for scalar conservation laws. *SIAM J. Numer. Anal.*, **48**(3): 1038–1063, July 2010.
- [53] T. Zhang, S. Yu. The derivative patch interpolation recovery technique and superconvergence for the discontinuous Galerkin method. *Applied Numerical Mathematics*, **85**: 128–141, 2014.
- [54] Z. Zhang. Ultraconvergence of the patch recovery technique II. *Math. Comput.*, **69**(229): 141–158, January 2000.
- [55] O.C. Zienkiewicz, J.Z. Zhu. A simple error estimator and adaptive procedure for practical engineering analysis. *International Journal for Numerical Methods in Engineering*, **24**(2): 337–357, 1987.
- [56] O.C. Zienkiewicz, J.Z. Zhu. The superconvergent patch recovery and a posteriori error estimates. Part 1: The recovery technique. *International Journal for Numerical Methods in Engineering*, **33**(7): 1331–1364, 1992.
- [57] O.C. Zienkiewicz, J.Z. Zhu. The superconvergent patch recovery and a posteriori error estimates. Part 2: Error estimates and adaptivity. *International Journal for Numerical Methods in Engineering*, **33**(7): 1365–1382, 1992.